iEnergy
REVIEW
https://doi.org/10.23919/IEN.2022.0029

The interfacial engineering of metal electrodes for high-specific-energy and long-lifespan batteries

Haomiao Li[1,2,†], Yi Shen[1,2,3,†], Zhuchan Zhang[2], Anran Cheng[2], Kangli Wang[1,2] ✉, Xianbo Zhou[1], Peng Cai[3], Yujie Zhang[3], Mengjun Li[3], Min Zhou[1,2], Wei Wang[1,2], Ruxing Wang[1,2] and Kai Jiang[1,2] ✉

ABSTRACT

High-specific-energy batteries with long-lifespan are the development aspiration for energy storage applications. Metal electrodes with high specific capacity and low reduction potential are potential candidates for next-generation high-specific-energy batteries. Nevertheless, the stability of the metal electrode batteries is constantly suffered from the unstable interface issue during the plating/stripping process, such as dendrite formation, dynamic evolution of solid electrolyte interphase, and other accompanied side reactions. To solve these challenges, numerous researches have been intensively studied based on the interfacial engineering of metal electrodes, including electrode configuration optimization, interfacial chemistry regulation and solid–solid interface construction, and the recent progress is elaborately introduced in this paper. Nevertheless, the dendrite issues cannot be entirely prohibited in solid metal electrodes, which motivate the search for potential alternatives. Liquid-metal electrodes with completely reversible structural changes and high mass transfer rate are rendered as an effective approach to solve the dendrite problem. Therefore, the development of liquid metal electrode batteries is reviewed in this paper, in which the interfacial issues are explicated and some commendable achievements are summarized. In the end, the implementation of interfacial engineering and the development roadmap of the metal electrode batteries are prospected.

KEYWORDS

Metal electrodes, interfacial engineering, metal dendrites, solid state batteries, liquid metal batteries.

The carbon neutrality has been the common goal of human society to realize sustainable development, which urges the transformation of traditional fossil-based energy resource to green energy consumption structures. Energy storage technology can efficiently integrate renewable energy into the grid and is a key support to achieve the goal of carbon neutrality. As one of the most potential energy storage technologies, lithium(Li)-ion batteries have had a deep influence on society, recognized by the 2019 Nobel Prize in Chemistry[1]. Although marvelous energy density has been achieved by graphite anode and lithium-metal oxide cathode, it is still limited to meet the demand of higher energy density. Metal electrodes have been explored as a potential alternative for their high theoretical capacity and low electrochemical potential[2,3]. The applications of metal electrodes in batteries have been studied for a long time, for example, Li-metal electrode in batteries was achieved by Laszczynski and Gorski in 1897[4]. However, the development of lithium-metal batteries has been put on hold due to the inability to solve the recharging issues of lithium-metal electrodes. Recently, the pursuit of high energy density has rekindled the researchers' interest in the field of metal electrodes.

Metal electrodes are charged and discharged through the electro-plating/stripping of metal ions, which is fundamentally responsible for the interface issue. The interface issues, including dendrite growth, evolution of the solid electrolyte interphase (SEI), and other side reactions, directly lead to the poor stability and safety of metal electrode batteries[5,6]. Fortunately, numerous solutions have been proposed in recent years, including electrode configuration optimization, interfacial chemistry regulation, solid–solid interface construction, and designing of liquid metal electrodes[7]. In this review, we summarize the original interface issues of metal electrode and some important influencing factors at first, as shown in Figure 1 (the ring layer in the middle). Then, the interfacial engineering efforts on metal electrodes are emphasized which includes the electrode configuration optimization, interfacial chemistry regulation, and construction of solid–solid interface. Moreover, the designing of liquid metal electrodes and the latest progress in metal electrode batteries are dedicated, including the enhancement of liquid metal electrodes wettability, the construction of stable liquid–liquid interface, and the measurement of the chemically stable interface. Finally, the prospects of various strategies in metal electrodes interface engineering are systematically reviewed, and the development direction of the next generation of high-specific-energy and long-lifespan metal electrode batteries is described.

1 Challenges of solid metal electrode in batteries

The interface characteristics of metal electrode directly determine the cycle life and safety of metal electrode batteries, which is one of the biggest challenges hindering its practical applications. The interface issues of metal electrodes could be attributed to three categories: dendrite formation, SEI evolution, and interface incompatibility and instability (as shown in Figure 2(a)). In

[1]School of Electrical and Electronic Engineering, Huazhong University of Science and Technology, Wuhan 430074, China; [2]State Key Laboratory of Advanced Electromagnetic Engineering and Technology, Huazhong University of Science and Technology, Wuhan 430074, China; [3]School of Material Science and Engineering, Huazhong University of Science and Technology, Wuhan 430074, China
† These two authors contributed equally to this work.
Address correspondence to Kangli Wang, klwang@hust.edu.cn; Kai Jiang, kjiang@hust.edu.cn

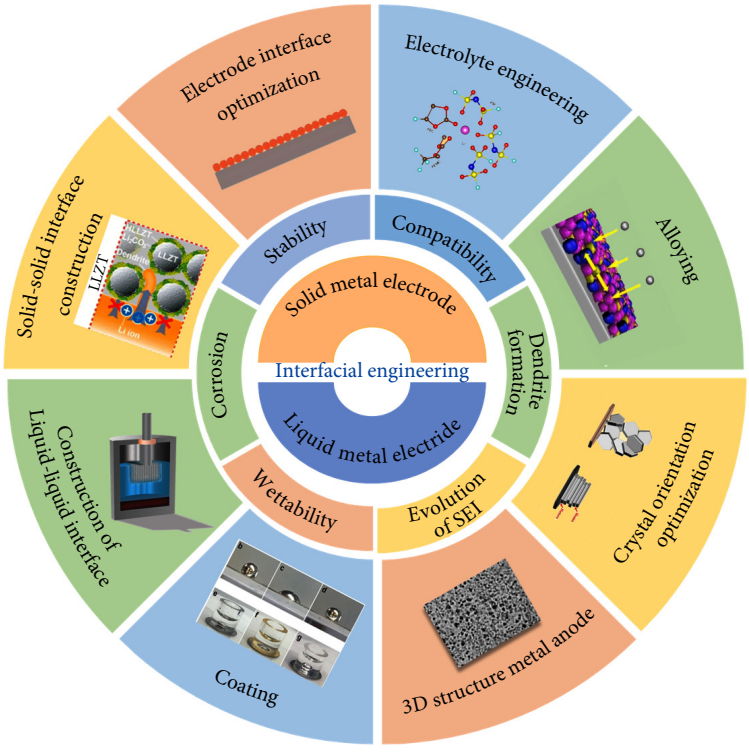

Fig. 1 An overview of the development of metal electrode batteries, including the interface issues of the solid metal electrodes and liquid metal electrodes (the ring layer in the middle), and responding interface engineering strategies (the outer ring layer).

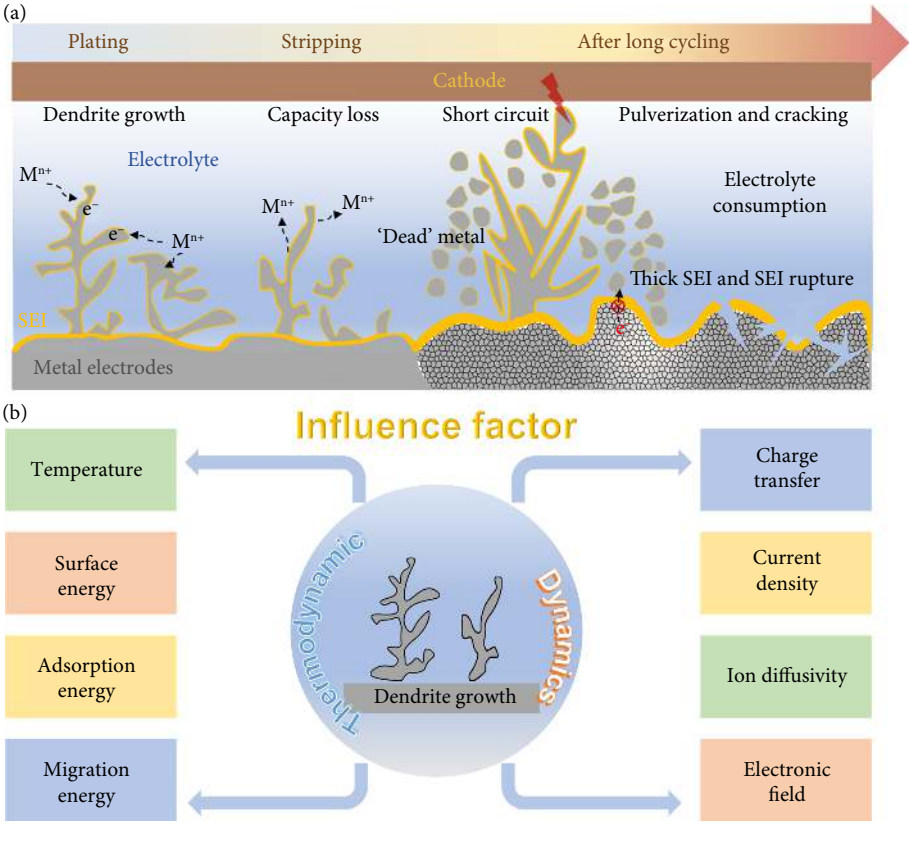

Fig. 2 (a) Schematic diagram of interface issues of solid metal anode. **(b)** Factors affecting dendrite growth.

Figure 2(a), the metal dendrites formed in electroplating process can easily detach from the substrate during the stripping process and form dead metals, which lead to the battery capacity fading. Moreover, the unrestricted growth of the metal dendrites can easily pierce the membrane and cause the battery short-circuit. In addition, the increased contact area caused by the dendrite will aggravate the consumption of the electrolyte, thus increasing the polarization and limiting the cycle life of metal electrode batteries.

1.1 Dendrite formation

In general, the deposition behavior of metal anodes can be classified into the nucleation and growth steps[1]. The favorable sites (defects such as impurities, cracks, pores, etc.) can effectively promote ions nucleation, inducing uneven ion accumulation on the metal substrate[2]. Similarly, the high current density will cause a non-uniform electric field on the surface of metal electrodes, and resulted in uneven ions nucleation. On this basis, metal ions tend to aggregate and grow into dendrites during the deposition process in order to decrease the surface energy and exposed area[3]. Therefore, The growth of dendrites is an electrochemical problem involving many complex factors inside the battery (Figure 2(b)), and there are also different interpretations for the formation of dendrites[4,5]. Take the lithium metal as an example, several models have been proposed, including the space–charge model[6], heterogeneous nucleation model[7], Sand's time model[8,9], etc. The most commonly accepted model is the space–charge model proposed by Chazalviel et al. to explain electrodeposition kinetics. In this model, they pointed out that the growth of Li dendrites in dilute solutions is fundamentally driven by the space charge formation when the anions near the cathode are depleted, and indicated that the time of the dendrite growth is proportional to the current density[6,8].

$$\tau = \pi D \frac{e^2 C_0^2 (\mu_a + \mu_{Li^+})^2}{4 J^2 \mu_a^2}$$

where τ is the initial time of dendrites growth (usually called Sand's time), J represents the current density, and D represents the diffusion coefficient. μ_a and μ_{Li^+} represent the mobility of anion and lithium ion, respectively. C_0 stands for the initial concentration of lithium ions. Sand's time equation lays strong support for the investigations and research in metal electrode batteries.

1.2 Dynamic evolution of SEI

As an electronic insulator and excellent ion conductor, SEI was first discovered by Dey and Sullivan in 1970[10] and defined by Peled in 1979[11], whose structure and composition are closely related to the deposition of metal ions. When the active metal electrodes are directly in contact with electrolytes, the reaction inevitably occurring at the electrode–electrolyte interface (EEI) will form SEI because of the low equilibrium potential of active metals (such as Li and Na). SEI is mainly composed of organic elements in the outer layer and inorganic elements in the inner layer[12]. Among them, the inorganic components are mainly M_xO_y, M_xF_y, $M_x(CO_3)_y$, and the organic components are mainly ROM, $ROCO_2M$, and RCOOM[13–18] (R is alkyl group and M is alkali metal ions). The diagram is shown in Figure 3(a).

Furthermore, the quality of the SEI film directly affects the electrochemical performance of batteries. A perfect SEI film should have the following concentrated characteristics: (1) physicochemical stability, (2) mechanical flexibility, and (3) efficient ions pathway. Shi et al. found that the SEI dynamically undergoes the formation and collapse process in Li-metal batteries[19]. Generally, metal ions deposition results in volume expansion of metal electrodes, and the consequent concentrated mechanical stress would destroy the integrity of SEI on the surface of metal electrodes. The breakage of the SEI film will expose the fresh metal electrode surface, which will constantly promote the consumption of the electrolyte and active materials, increasing the interface charge transfer resistance and the polarization (Figure 3(b)).

1.3 Interfacial incompatibility and instability

The use of non-flammable solid-state electrolytes (SSEs) and aqueous electrolytes can alleviate the potential safety hazard caused by thermal runaway of batteries resulted from dendrites, and improve the safety of metal electrode batteries. However, the concomitant problems in solid-state batteries and aqueous electrolyte batteries should be concerned when pairing with the metal electrodes.

For solid-state batteries, the stable electrochemical operation has been greatly hindered by the interfacial incompatibility and instability at the solid-state-electrolytes/metal electrodes interface. Firstly, the lattice mismatch between the electrode and SSEs will result in a huge contact loss and limit the discharge performance of the solid-state battery[20,21]. Besides, high reactive metal electrodes can reduce the SSEs to form interphase and the electron-conductive interphase, in turn, this process will promote the constant decomposition of SSEs[22]. These phenomena would lead to dendrites growth, increasing polarization, poor kinetics of SSEs, and capacity fading of the battery.

In addition, aqueous electrolyte systems have also been extensively studied in recent years, the most typical of which is aqueous zinc-ion batteries. Generally, the electrochemical reaction in aqueous zinc-ion batteries is carried out in the weakly acidic electrolyte in which the hydrogen evolution reaction (HER) and corrosion of zinc metal electrodes will inevitably occur[23]. In addition, the HER will lead to the formation of electrochemically active by-products (like $ZnSO_4[Zn(OH)_2]_3{\cdot}xH_2O$). These side reactions will constantly consume electrolyte and active zinc and deteriorate the battery performance.

2 Interfacial engineering of solid metal electrodes

The operation of a battery is always accompanied by electron

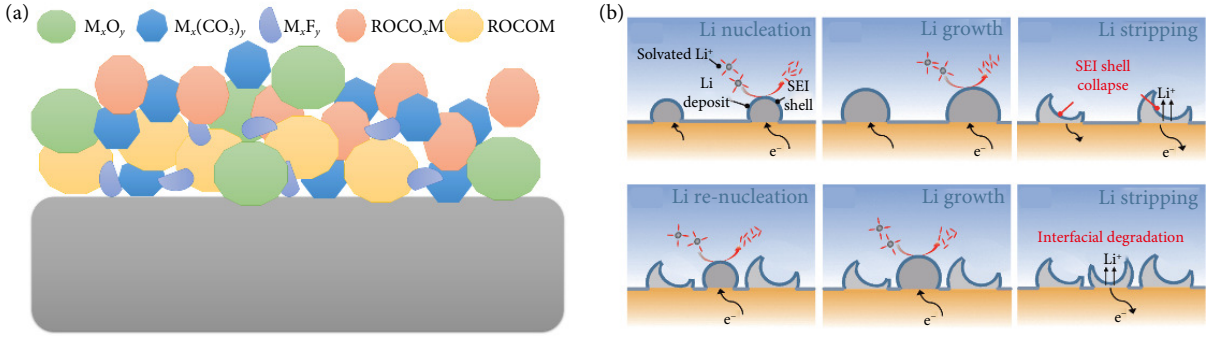

Fig. 3 **(a)** The composition of SEI. **(b)** Schematic diagram of SEI evolution during Li deposition/stripping at electrode/electrolyte interface (reprinted with permission from ref. [19], © Science China Press and Springer-Verlag GmbH Germany, part of Springer Nature 2021).

transfer and ion transmission at the EEI. A stable EEI plays a vital role in promoting cyclability and extending the lifetime of rechargeable metal electrode batteries. Many measurements have been put forward which can be divided into the intrinsic transport dynamics optimization of the metal electrode, interfacial chemistry regulation, and the solid–solid interphase construction.

2.1 Intrinsic transport dynamics optimization

Regulating the ion transport dynamics has been proven to be an effective strategy to inhibit dendrite formation. Based on lowering the nucleation energy barrier, exposing nucleating sites, and reducing the volume expansion, several manipulating strategies can be categorized in the 3D structured metal anode, regulating the crystal orientation and alloying. A brief summarization is shown in Table 1.

2.1.1 3D structured metal anode

The unique integrated network in 3D architecture can favor the ions/electrons transportation, provide more nucleation sites, minimize the local current density and accommodate volume changes[24,25]. However, the structure modification of pure metals may suffer from structural destruction and is difficult for the large-scale manufactory[3]. Therefore, the focus has been shifted to optimizing the 3D metal and carbon-based current collector of alkali metal electrodes.

Mountainous porous metal current collectors (Cu foam, Ni foam, porous Al[26], etc.) have been applied in metal electrodes and have been confirmed to extend the cycle life and improve the CE (Figures 4(a)–4(d))[27]. Porous Cu current collectors have been applied in multiple metal electrodes. Zhang et al.[28] introduced 3D porous Cu (3DCu@NG) current collector in lithium-metal anodes. The Li–3DCu@NG anode presents a high areal capacity of 4 mAh·cm^{-2} and an ultralow voltage hysteresis of ≈19 mV. Sun et al.[29] utilized $Cu_{0.7}Zn_{0.3}$ tape to fabricate a 3D porous Cu current collector in zinc ion batteries, realizing a high coulombic efficiency (CE) of 99.4% after 400 cycles at 1 mA·cm^{-2} and low voltage hysteresis voltage (20 mV).

3D carbon-based current collectors have stood out among all metal current collectors due to the lightweight, easy processing, and low-cost merits. Many 3D carbon-based current collectors like carbon cloth, porous carbon, 3D carbon nanotubes(CNTs), 3D graphene have been widely investigated. Graphene frameworks composed of 3D hollow spheres have been reported as a free-standing host for the smooth deposition of Li ion[30]. The optimized Li metal electrode can stably operate over 1000 h and the LFP||3D-GF@Li full cell exhibits the capacity retention of 90% for 200 cycles. 3D carbon scaffold with Zn metal is often synthesized by depositing Zn onto the 3D framework. The as-fabricated anode presents a promisingly low voltage hysteresis (27 mV) and ultra-stable cyclability (200 h at 2 mA·cm^{-2}).

The introduced 3D metal and carbon-based current collectors are widely researched to mitigate the dendrite problems in metal electrodes. However, the high electrolyte consumption and the low initial CE of the 3D current collector hinder their further

Table 1 Strategies in intrinsic transport dynamics optimization

Modification methods	Systems	Configuration	Current density (mA·cm^{-2})/ areal capacity (mAh·cm^{-2})	Plating-stripping cycles of metal electrode	Cycling life in full battery	Ref
3D structured metal current collectors	Li	3D Cu mesh@CuO	10/3	1000 cycles	1000 cycles, 77.6%	[33]
		3D Ni foam@$NiCo_2O_4$ nano-rods	1/1	500 cycles	—	[34]
		3D porous Au/ Cu nano-scaffold	1/1	1300 h	200 cycles, 97.7%	[35]
		Gradient conductive-dielectric framework	1/8	1040 h	100 cycles, 99.4%	[36]
	Na	Oxsygen-treated Cu foam	2/3	300 h	100 cycles, 87%	[37]
	Zn	3D Zn	0.5/0.1	1400 h	—	[38]
		3D Cu foam@Zn–Sn–Pb alloy	4/1	1000 h	4000 cycles, 87%	[39]
3D carbon-based current collectors	Li	Nitrogen-doped graphitic carbon foams	2/1	1200 h	300 cycles, 99.6%	[40]
		MOFs modified carbon cloth	2/4	1000 h	200 cycles, 75 %	[41]
	Na	Carbonized coconut framework	50/1	400 h	100 cycles, 94%	[42]
		3D flexible carbon felt	5/2	120 cycles	200 cycles, 98.6%	[43]
	Zn	3D CNT	2/2	200 h	—	[44]
		3D porous hollow fiber scaffold@TiO_2, SiO_2, and carbon	20/1	2000 cycles	1000 cycles, 85%	[45]
Regulating crystal orientation	Li	Cu(100) current collector	4/1	200 cycles	—	[46]
	Zn	(002) Zn	16/0.8	10000 cycles	—	[47]
		(100) Zn	5/1	1200 h	—	[48]
Alloying	Li	Li–Al alloy	0.5/1	1700 h	280 cycles, 80%	[52]
		Li–Bi, Li–In, Li–Zn alloy	2/2	1000 h	1500 cycles, 87%	[49]
	Na	Na–Ge alloy	15.83/—	15 cycles	—	[50]
	Zn	Zn–Cu alloy	4/1.58	5000 cycles	5000 cycles, 90.2%	[51]

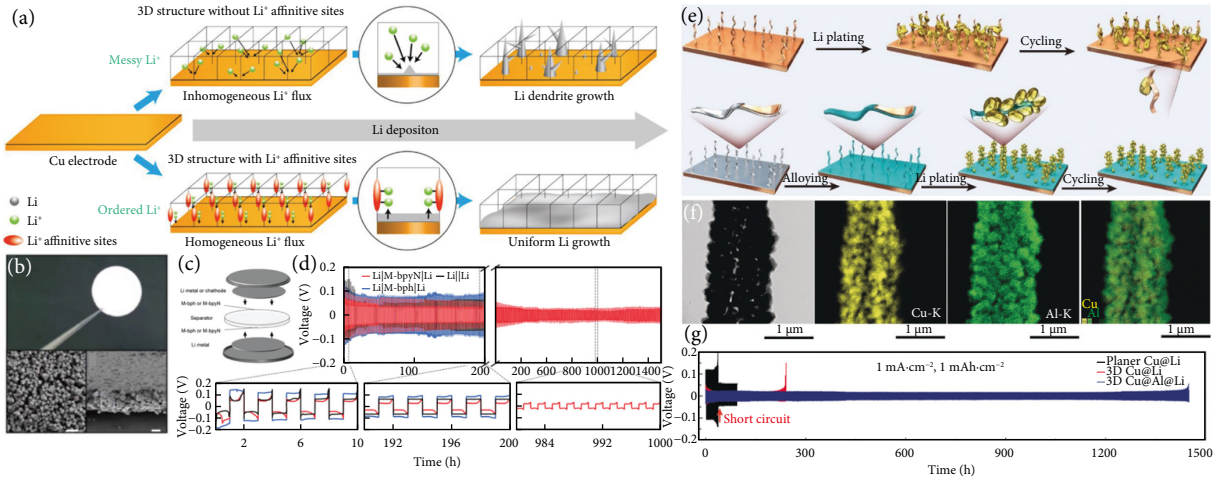

Fig. 4 **(a)** Diagram of inhomogeneous and homogenous Li flux on Cu current collectors. **(b)** SEM image of M-bpyN@Cu. **(c)** Schematic of cell assembling using M-bpyN layers. **(d)** Charge-discharge profile of Li||Li, Li|M-bph|Li, and Li|M-bpyN|Li for long-term cycling at a current density of 1.0 mA·cm^{-2}. (a–d) Reprinted with permission from ref. [27], © 2020 The Authors. **(e)** Schematic of the Li plating process on the 3D Cu foil and 3D Cu@Al foil. **(f)** Bright-field TEM (STEM) image and the corresponding Cu, Al, and overlapped element mapping images of the 3D Cu@Al foil. **(g)** Voltage profiles of metallic Li plating/stripping in three styles of symmetric cells (planar Cu@Li, 3D Cu@Li, and 3D Cu@Al@Li) at 1 mA·cm^{-2} for 1 mAh·cm^{-2}. (e–g) Reprinted with permission from ref. [52], © 2019 Wiley-VCH Verlag GmbH&Co. KGaA,Weinh.

application[31]. Moreover, the fabrication cost is too high, and the mechanical strength and thickness of the 3D structured metal electrode are insufficient for practical usage[32].

2.1.2 *Regulating the crystal orientation*

According to the preferential ion transferring path, intentionally exposing the preferred orientation crystal plane can reduce the ion nucleation energy barrier and guide the ion transfer, thus prohibiting ion accumulation and dendrite formation. In crystallography study, lithium-ion has been proven to deposit favorably in <110> direction. Therefore, the specifically oriented substrate is advisable to guide Li-ion transportation. Furthermore, considering the ions can easily transfer along the [110] plane in sodium metal batteries, Al substrate is preferable. Further examples can be seen in Table 1[33–52]. Nevertheless, the in-depth investigation of crystal orientation manipulation is still lacking, and further research is encouraged to be brought about. If the matured fabrication process is established, a brand-new century will be opened for metal batteries.

2.1.3 *Alloying*

Alloying can ameliorate the binding energy barrier, thus preventing the dendrite growth and alleviating the metal corrosion. Ye et al.[52] found that the Li–Al alloy layer could stably cycle over 300 cycles (Figures 4(e)–(g)). Through pre-loading alloying elements on the current collector substrate, Li and other metals can uniformly deposit on the surface. For sodium metal batteries (Na–Sn, Na–Sb, Na–Pb, and Na–Ge alloy) and zinc-metal batteries (Zn–Cu, Zn–Al, etc.), fabricating intermetallic compounds is also a vital modification strategy in enhancing the battery performance.

Nonetheless, there are still some problems with alloying strategy. The nucleation of metal and the growth of metal will be effectively influenced the surface and the SEI film of metal alloy. Also, the volume expansion exists in several alloys during alkali-ion insertion/departure (Li_xSi, KSn, K_3Sb[53], etc.).

2.2 Interfacial chemistry regulation

Interfacial chemistry regulation is one of the most efficient strategies for constructing a stable EEI discussed in Section 2.2. Rational designing the interfacial chemical components, optimizing the electrolyte and artificial SEI films which can adapt to various physicochemical environments might efficiently stabilize the metal electrode battery operation.

2.2.1 *Electrolyte optimization*

Optimizing the electrolyte components can effectively stabilize the metal electrode SEI. Thermodynamically, electrolyte components with lower LUMO energy and higher redox potential will be prior reduced, thus stabilizing the electrode-electrolyte interface. Due to the high electronegativity, ionic potential, and low polarizability of fluorine atoms, fluorinated solvents might be one of the most promising strategies for metal electrodes. By replacing the hydrogen atom with fluorine, the HOMO and LUMO energy levels of solvents could be decreased, which not only facilitates the formation of effective SEI layers but also broadens the electrochemical window[54]. As a typical partially fluorinated solvent, fluoroethylene carbonate (FEC) has been widely applied as the film-forming additive in Li-ion batteries, owing to its lower LUMO (−0.87 eV)[55]. Recently, based on the ether-based electrolyte's excellent reduction stability and the fluorinated strategy, Yu et al. reported a new type of fluorinated ether solvent 1,4-dimethoxylbutane (FDMB), which possesses superior anode compatibility and high-voltage stability (Figure 5)[56]. Further, they designed another fluorinated ether solvent 1,6-dimethoxyhexane (FDMH), which has a longer -CF_2- backbone than FDMB[57]. With the 1, 2-dimethoxyethane (DME) co-solvent, the fluorinated ether electrolyte exhibits a CE of 99.5% without dendrite formation and shows excellent oxidative stability under 6 V, revealing the feasibility of the fluorinated strategy.

Based on the dendrite growth depletion model (Eq. (1)), highly concentrated electrolytes (HCEs, usually > 3 M) would increase the threshold of J, thus the dendrite growth could be dramatically suppressed[58]. In HCEs, the LUMO energy is mainly dominated by salt anions which will be reduced before the solvent at the metal electrode surface and form an anion-derived SEI[59]. Up to now, a series of electrolyte salts with novel anions have been investigated[60–63], among which the salt with FSI^- anion has drawn

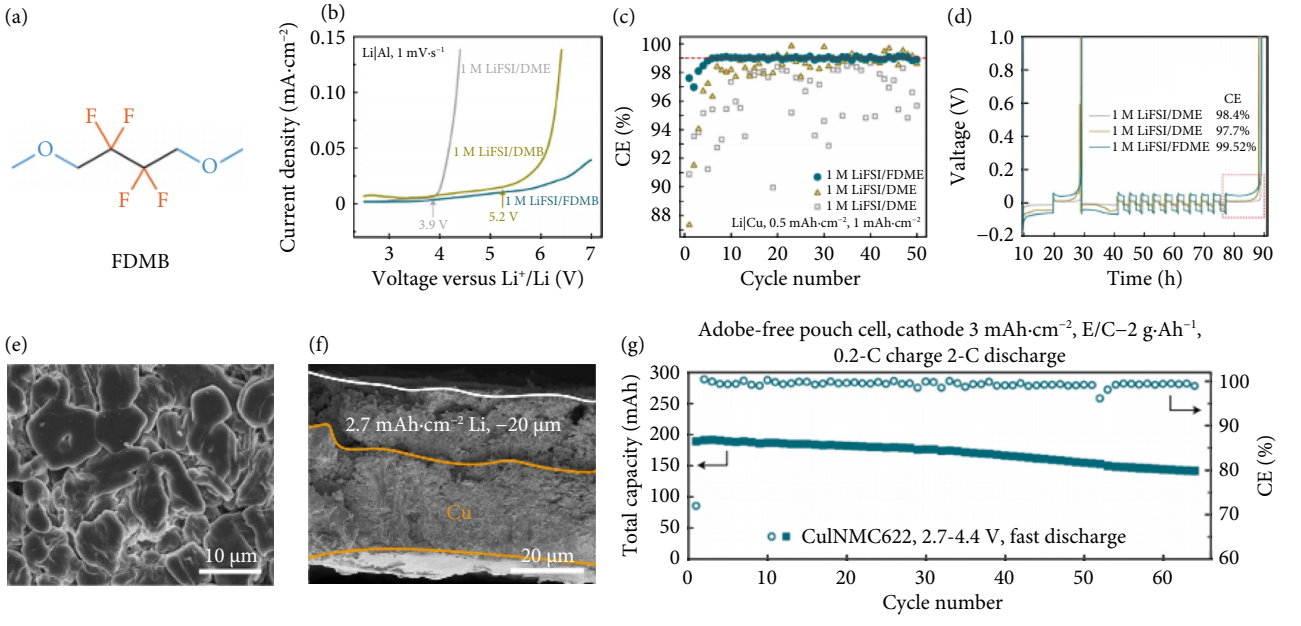

Fig. 5 **(a)** The molecular structures of FDMB. **(b)** The oxidation stability of three electrolytes in Li||Al half cells. **(c,d)** The cycling and CE of Li||Cu half cells using different electrolytes. **(e,f)** Li morphology in 1 M LiFSI/DMB after 70 cycles. **(g)** The full battery performance of anode-free Cu||NMC622 pouch cell with 1 M LiFSI/DMB electrolyte. Reprinted with permission from ref. [56], © The Author(s), under exclusive licence to Springer Nature Limited 2020.

much attention due to its excellent anode compatibility. The FSI salts are thermodynamically unstable at dilute concentrations but can form a stable solvated structure when their concentration increases to 4 M[64–66]. Although HCEs provide a route for stable metal anodes, low ionic conductivity, poor wettability, high viscosity of the electrolyte, and the high expense are needed be considered. To overcome the shortcomings of HCEs, localized high-concentration electrolytes (LHCEs) are further developed[67]. With the "inert" diluent added into the HCEs, the surrounding environment of metal cations could be significantly retained[68].

By regional design reactants in the electrolytes, the EEI stability could be considerably enhanced. The metal electrode interface chemistry could be largely optimized by combining the fluorinated electrolyte solvents with nonfluorinated counterparts. Meanwhile, the effect of different salts is also crucial and the concentration strategy provides a novel view to facilitate the formation of effective SEI layers.

2.2.2 *Electrode interface optimization*

Owing to the coarse, fragile, and inhomogeneous features of pristine SEI, artificial SEI films can act as a compact layer adhering well to the metal and is elastic and flexible enough to prevent metallic penetration and alleviate the volume change during repeated cycles[69]. The artificial SEI can be divided into the inorganic and organic interface layers, which will be further introduced in the following paragraph.

The inorganic interface layer is initially grafted onto the electrode by mechanical coating[70,71], which is characterized by convenience, low cost, and heavily relying on adhesives (such as polyvinylidene fluoride). Considering the interface thickness and structure maintaining, atomic layer deposition (ALD) can simultaneously achieve nanoscale thin film with ultra-precise thickness control and atomic-level compactness[72]. Zhao et al. reported an ALD inorganic interface protection method by fabricating an ultra-thin Al_2O_3 artificial film to protect Na metal anodes[73]. By introducing the artificial film, Na@Al_2O_3–Na@Al_2O_3 symmetric cells could provide a stable stripping/plating behavior within 100 h at 3 mA·cm^{-2} and cycle at 5 mA·cm^{-2} for about 75 h. In addition, the TiO_2 interface layer has been reported to deposit on the Zn electrode with an ultra-low thickness of 8 nm and a regular texture (Figures 6(a)–6(d))[74]. This ALD interface layer is compact enough to reduce the exchange current density in the aqueous electrolyte, maintain a relatively stable pH medium, and allow uniform deposition during repeated cycles. Despite these advantages, the application of the ALD method is still hindered by its high cost and other promising technologies need to be explored[75].

Nevertheless, the application of inorganic artificial SEI film is still partially restricted. For example, because of the low melting point of K, there are no reports on ALD coatings. In addition, recent studies have pointed out the potential of organic layers. The delicate interfacial coupling between the organic layer and the metal electrode can significantly reduce the ion interface transfer resistance. Gao et al. reported the reactive polymer composite (RPC) based on poly(vinylsulfonyl fluoride-ran-2-vinyl-1,3-dioxolane) (P(SF-DOL))-graphene oxide (GO) nanosheets[76]. The solution containing the material was cast onto the surface of the lithium metal, and then the material reacted with the lithium metal to form a chemically harmonious SEI interface (Figures 6(e) and 6(f)). More importantly, Li-metal batteries with RPC SEI can cycle with high CE (99.1%) under high area capacity (4 mAh·cm^{-2}). These results indicate that, if properly designed, organic-rich SEI can be used as an excellent interfacial stabilizer for lithium-metal anodes (Table 2)[36,77–86].

2.3 Solid-solid interface construction

Intrinsically safe and high-modulus inorganic SSEs have been proposed as the potential electrolyte for metal electrode batteries. The mechanical modulus of most SSEs is much higher than that of alkali metal electrodes, rendered to suppress the dendrite formation promisingly[87–89]. On the other hand, the single-ion-conducting feature of inorganic SSEs can circumvent the concentration polarization induced by anion migration in the liquid electrolyte. However, there are still some interfacial instability and compatibility problems existing to be solved before their further application. Several strategies are summarized in Table 3[90–97].

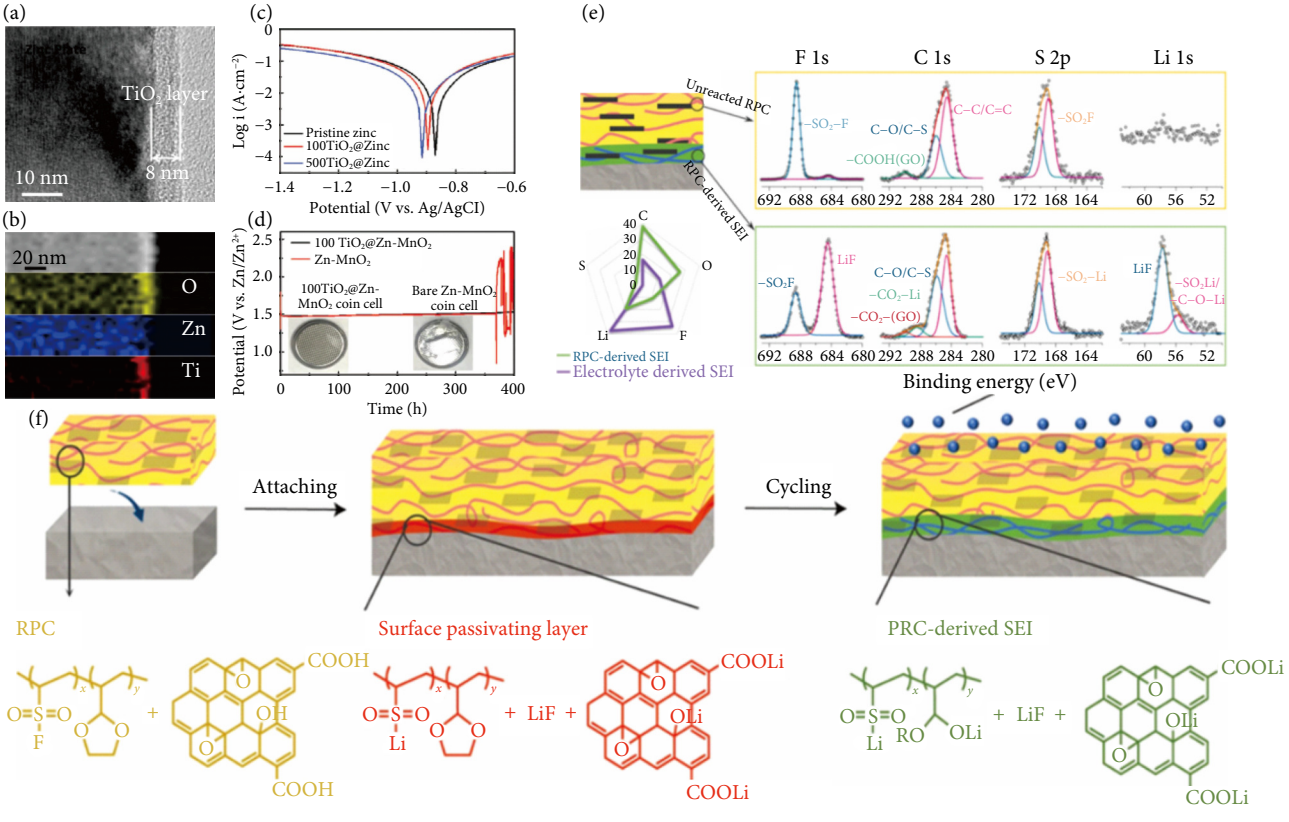

Fig. 6 **(a,b)** SEM and the mapping images of the inorganic TiO_2 interface layer. **(c)** Corrosion curves of mental-based Zn anode improved by inorganic TiO_2 interface layer. **(d)** Self-discharge curves of full cells with and without inorganic interface layer ALD method. (a–d) Reprinted with permission from ref. [74], © 2018 Wiley-VCH Verlag GmbH&Co. KGaA,Weinh. **(e)** The reaction sequence and SEI structure after cycling, **(f)** schematic illustration of RPC structure. (e,f) Reprinted with permission from ref. [76], © The Author(s), under exclusive licence to Springer Nature Limited 2019.

Table 2 **Recent advances adopting artificial SEI films for electrode interface optimization**

Strategies	Systems	Configuration	Current density (mA·cm^{-2})/ areal capacity (mAh·cm^{-2})	Plating-stripping cycles of metal electrode (cycles)	Cycling life in full battery	Ref
Inorganic interface layer	Li	CNT with ZnO	10/1	500	200 cycles, 54%	[77]
		Cu ionic gradient	1/1	2100	300 cycles, 79%	[78]
	Na	Sn interlayer	0.5/0.5	500	50 cycles, 80%	[79]
		NaBr coating	1/1	250	—	[80]
		MXene/CNT	0.5/0.5	200	500 cycles, 74%	[81]
	K	rGO-3D Cu	1/0.5	100	—	[82]
		Hg-alloy layer	0.2/0.2	300	240 cycles, 80%	[83]
	Zn	$NaTi_2(PO_4)_3$	1/1	240	10000 cycles, 80%	[84]
Organic interface layer	Li	Melamine	1/1	400	100 cycles, 99.4%	[36]
	Na	Alucone	3/1	180	—	[85]
	Zn	Konjac glucomannan	0.2/0.2	900	5000 cycles, 98.8%	[86]

2.3.1 *Optimized solid-solid interfacial stability*

Because of the fragileness of SSEs, it is better to pre-anneal the metal to the molten state, which would alleviate the lattice mismatch issue. However, a clean and smooth interface surface is hard to achieve for solid-state batteries. On the one hand, the impurity on SSEs or electrodes is usually randomly distributed and has a weak connection with the substrates, which highly decreases the wettability. On the other hand, the poor ionic conductivity of impurity would impede ion transfer throughout the interface.

To improve the interfacial contact and kinetics, various artificial interlayers with better wettability for metallic Li are introduced. Li et al. introduced subtle carbon to react with Li_2CO_3 on the garnet SSEs in Ar at 700 °C and significantly reduced the interfacial resistances to 28 Ω·cm^2 (Figure 7(a))[98]. Apart from improving interfacial contact, the interlayer can facilitate the ion-conducting at the interface and block the electron infusion. Huo et al. coated garnet SSEs with polyacrylic acid (PAA) polymer, which can react with Li to in situ form a flexible Li-inserted PPA interlayer to both relieve interfacial stress and prohibit electrons infusion (Figure 7(b))[99]. Consequently, the Li symmetric cells assembled with PAA-coated garnet SSEs can cycle stably at 1 mA·cm^{-2} over 400 h. Cheng et al. synthesized a crystalline sulfonated-covalent

Table 3 Efforts on solid–solid interphase construction

Issues	Methods	Strategies	Interfacial impedance (Ω·cm²)	Current density (mA·cm⁻²/h)/ lifetime (h)	Areal capacity (mAh·cm⁻²)	Ref
Interfacial instability	Removing the surface impurity of SSEs	High-temperature calcination	49	0.3/200	0.3	[90]
		Acid-salt treatment	11.6	0.5/1000	0.25	[91]
	Constructing 3D electron/ ion conducting network within metal electrode	3D-micropatterned LLZO	39.5	0.5/500	0.5	[92]
		Porous NZSP framework	175	0.3/400	0.15	[93]
	Interfacial modification	Li_3N/LiF interphase	15.3	1/220	1	[94]
Interfacial incompatibility	Doping	O-doped Li_6PS_5Cl	160	1/600	0.1	[95]
		F-doped Li_6PS_5Cl	130	6.37/250	5	[96]
		N-doped Li_6PS_5Cl	—	1/200	1	[97]

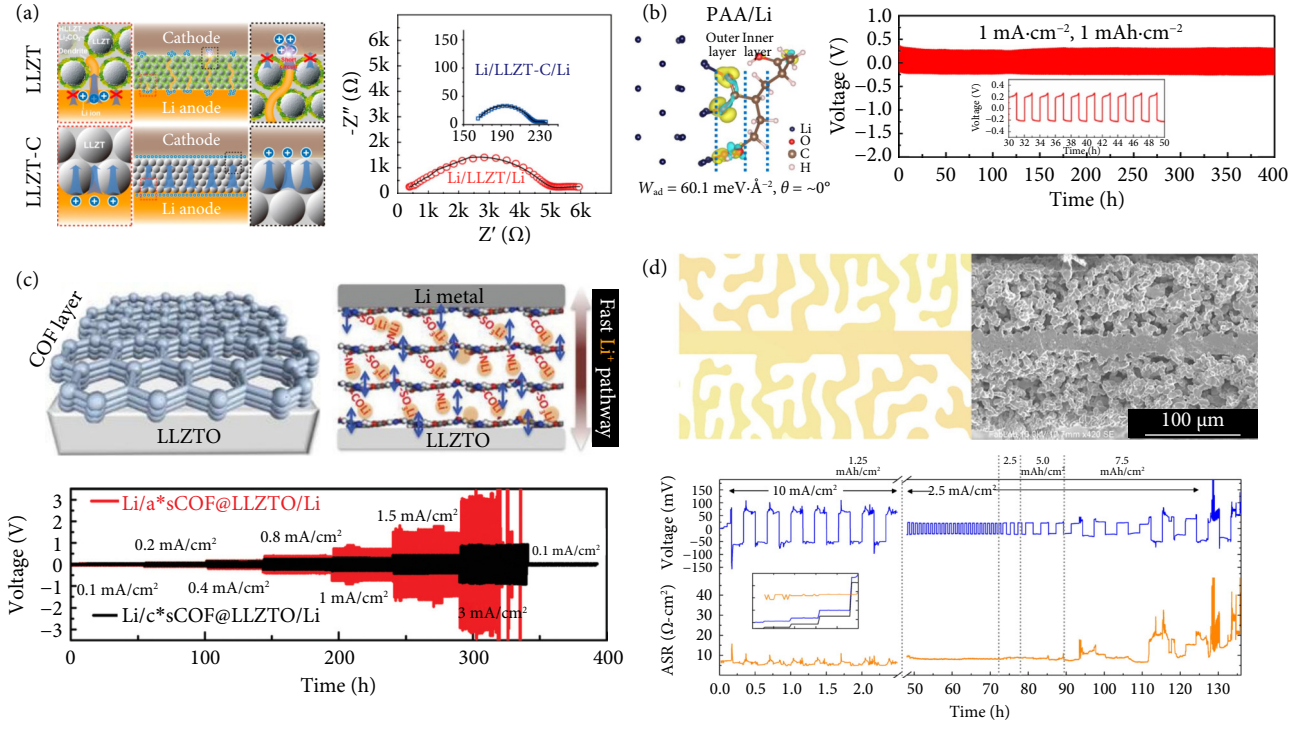

Fig. 7 **(a)** Schematic of the interface between Li-metal and garnet LLZT/LLZT-C, the electrochemical impedance of Li/LLZT/Li and Li/LLZT-C/Li cells (reprinted with permission from ref. [98], © 2018 American Chemical Society). **(b)** The structure and charge transfer at PPA/Li interfaces and the cycling performance of Li/PPA-coated LLZTO/Li cells (reprinted with permission from ref. [99], © The Author(s) 2021). **(c)** Schematic of self-assembly of COF on garnet SSE and Li^+ transfer in the COF layer and the cycling performance of Li/COF@LLZTO/Li and Li/COF@LLZTO/Li cells at various current densities (reprinted with permission from ref. [100], © 2020 Wiley-VCH Verlag GmbH&Co. KGaA,Weinh). **(d)** Schematic of porous-dense-porous trilayer structure of LLZTO and corresponding cross-sectional SEM images, cycling performance of Li/Li symmetric cells assembled with trilayer structure at different current density and area capacity (reprinted with permission from ref. [101], © 2018 Elsevier).

organic framework (COF) thin layer on the garnet SSEs surface through a simple solution process (Figure 7(c))[100]. Lithiated COF interlayer can prominently improve the lithiophilicity of garnet electrolytes and create the pathway for effective Li^+ diffusion, accompanied by which the Li/COF@LLZTO/Li cells can cycle at an ultrahigh current density of 3 mA·cm⁻².

Unlike the liquid electrolyte systems, the rigid SSEs are incapable of self-adapting to the huge volume expansion of metal electrodes, ultimately resulting in poor contact. The interdigital or three-dimensional structure of SSEs is promising to accommodate the stress generated in metal electrodes, increase the SSEs/metal electrode interfacial surface area and relieve local current density concentration. Hitz et al. designed a 3D Li-garnet-electrolyte architecture via a template method and achieved a 40 fold expanded SSEs/metal electrodes interface for prohibiting the dendrite even at an ultrahigh current density of 10 mA·cm⁻² (Figure 7(d))[101].

2.3.2 *Improved interfacial compatibility*

In addition to the common interfacial instability, the interfacial incompatibility between SSEs and metal electrodes would induce the growth of the interphase. Once the interphase is electronically conducting, the electron would transfer through it to reduce the metallic cation in SSEs and result in high interface resistance and Li dendrite growth. To avoid the continuous attack from electrons under the reduction potential, it is necessary to construct artificial interphase to separate SSEs and metal electrodes and provide channels for ionic transfer.

The simplest and most scalable strategy is to passivate the metal electrodes. The passivation layer needs to be highly ionic conducting for fast ionic diffusion but electronic insulating for suppressing any electrochemical reduction of SSEs and is as thin as possible for low resistance. There are three ways to obtain such a passivation layer: pre-treating the metal electrodes, inserting the as-prepared functional layer at the SSEs/metal electrode interface, and modifying the component of SSEs. Wan et al. added LiTFSI–$Mg(TFSI)_2$–DME liquid electrolyte between $Li_{10}GeP_2S_{12}$(LGPS) SSEs and Li-metal electrode to form a bifunctional Li_xMg/LiF/polymer interphase and avoid the reduction of LGPS by Li metal (Figure 8(a))[102]. In addition, the lithiophilic Li_xMg alloy at the Li electrode side contributes to guiding Li plating under interphase and the lithiophobic and electron insulating LiF at the LGPS side help to avoid the reduction of LGPS and the formation of Li dendrites. Zhang et al. doped Li_2O into Li_6PS_5Br argyrodite SSEs (Figure 8(b))[103]. Even though direct contact with the molten Li, the oxygen-doped Li_6PS_5Br shows no significant exothermic reaction, indicating a positive reaction free energy (ΔG) at room temperature and excellent compatibility between oxygen-doped Li_6PS_5Br and Li electrode.

In summary, despite the high modulus, expanded electrochemical window, and single-ion-conducting merits, there are still some problems such as physical contact loss and parasitic reactions for SSEs need to be solved before commercialization. The strategies targeted to boost the interfacial stability and compatibility between SSEs and metal electrodes will continue to be the focus of researchers.

3 Interfacial engineering of liquid metal electrodes

Liquid metal electrodes with the merits of high fluidity and rapid mass transfer process can effectively solve the dendrite growth and structure collapse in solid metal electrodes. Therefore, the liquid metal electrode has been widely investigated, the typical applications in which are liquid metal batteries (LMBs), sodium–sulfur (Na–S), and ZEBRA batteries[104]. However, the practical applications of liquid metal electrodes still face interfacial challenges. First, liquid metals have high surface tension and poor wettability with collectors or solid electrolytes. Second, the melting point of metals is usually above 200 °C, which requires a high operating temperature (>300 °C). Under such conditions, the long-term sealing and corrosion issues of batteries need to be considered. To alleviate the above mentioned problems, numerous efforts have been made but some challenges are still remarkable, which are summarized in Table 4[105–120].

3.1 Wettability of liquid–solid interface

The unsatisfying wettability of liquid metal could hinder the ion and electron transfer and increase the internal resistance of the battery. At present, alloying and coating strategies are invented to solve this problem.

3.1.1 *Alloying*

The strong bonding force between alloying elements and the solid electrolytes can reduce the superficial internal energy and optimize the wettability of liquid metal electrodes. Alloying strategy was first used to improve the wettability of liquid metal sodium anode and solid electrolyte in Na–S battery and ZEBRA battery. Lu et al. studied the wettability of Na–K, Na–Rb, and Na–Cs alloys on β"-Al_2O_3 electrolytes, which found that all three alloys can effectively improve the wettability (Figure 9)[106]. Due to the strong interaction between Cs atoms and β"-Al_2O_3 electrolytes, the wettability of the liquid metal electrode-solid electrolyte interface has been significantly improved, and the Na–S battery with Na–Cs alloy can be operated stably at 150 °C. In addition to the use of alkali metals, some low melting point metals such as Bi, Sn, In, etc. are also chosen as alloying elements despite their low solubility in liquid Na(1~2 wt%)[121].

3.1.2 *Coating*

Coating a modified layer on the solid electrolytes can change the contact characteristics of liquid metal electrodes, and improve the wettability of liquid metal electrodes. In Na–S and ZEBRA batteries, researches have shown that coating Pb[122], Sn[121], Bi islands[123], Pt grid[124], Ni nanowires[125], porous iron oxide[126], and graphene layer[127] on the surface of the β"-Al_2O_3 electrolytes can greatly enhance the wettability of liquid Na metal electrodes. Li et al. adopted lead acetate trihydrate to treat the surface of β"-Al_2O_3 electrolytes, and the Na–S battery can stably operate for more than 1000 cycles at a working temperature as low as 120 °C[128]. Gross et

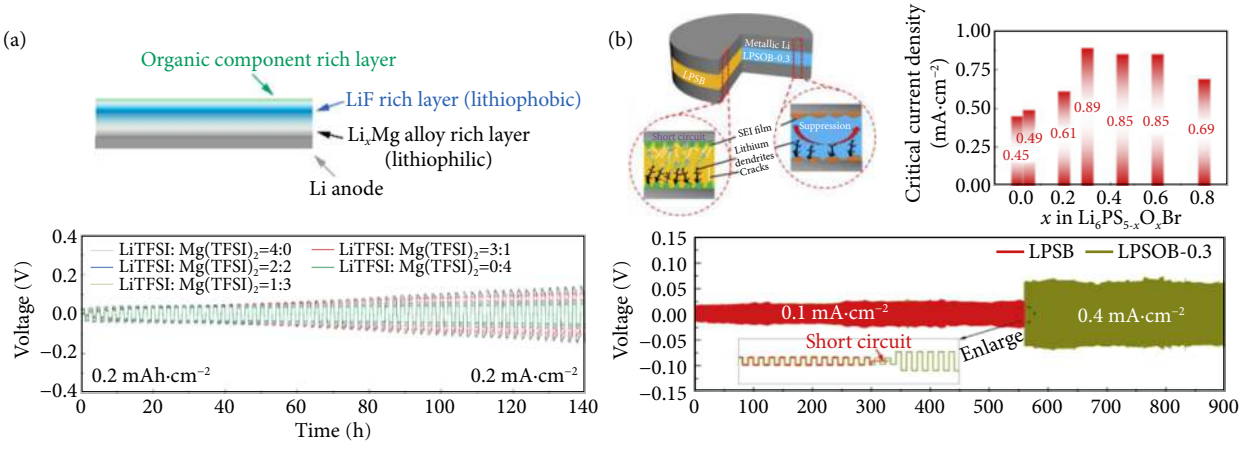

Fig. 8 **(a)** Illustration of in situ formation of the Li_xMg/LiF/polymer solid electrolyte interphase between Li and LGPS and galvanostatic cycling of the Li/LGPS/Li cell using different LiTFSI–$Mg(TFSI)_2$–DME-treated LGPS (reprinted with permission from ref. [102], © 2021 American Chemical Society). **(b)** Schematic of the excellent dendrite suppression capability for LPSOB-0.3 in contrast to LPSB, the critical current density of the Li/$Li_6PS_{5-x}O_xBr$ symmetric cells and galvanostatic cycling of Li/LPSOB-0.3/Li and Li/LPSB/Li cells (reprinted with permission from ref. [103], © 2019 Elsevier B.V.).

Table 4 The applications and challenges of liquid metal electrode batteries

Interface type	Liquid metal electrodes	Electrolytes	Operating temp. (°C)	Battery capacity (Ah) and areal capacity ($mAh·cm^{-2}$)	Cycle life and capacity retention	Issues	Ref
Liquid–solid	Na	β"-Al_2O_3	350	30,—	1200 cycles,—	Solid electrolyte membranes are brittle and difficult to be fabricated	[105]
	Na–Cs	β"-Al_2O_3	150	— ,—	100 cycles, 97%		[106]
	Na	NASICON	110	0.025,—	400 cycles, 100%		[107]
	Li||Sn–Pb	LLZTO	240	0.6, 600	120 cycles,—		[108]
	Li||Bi–Pb	LLZTO	240	0.38, 380	80 cycles, —		[108]
Liquid–liquid	Mg||Sb	KCl–NaCl–$MgCl_2$	700	2, 500	<10 cycles, 94%	High operating temperature, sealing and corrosion issues at enhanced temperature	[109]
	Li||Sb–Pb	LiF–LiCl–LiI	450	1.9, 600	450 cycles, 96.7%		[110]
	Li||Sb–Sn	LiF–LiCl–LiBr	500	20, ~850	430 cycles, 100%		[111]
	Li||Sb	LiF–LiCl–LiBr	550	30, 1060	470 cycles, 100%		[112]
	Li||Bi	LiF–LiCl	550	130, ~750	300 cycles, 100%		[113]
	Li||Bi–Sb	LiF–LiCl	550	3, 160	160 cycles, 80%		[114]
	Li||Bi–Sb–Sn	LiF–LiCl–LiBr	500	0.8, -	1000 cycles, 100%		[115]
	Li||Te–Sn	LiF–LiCl–LiBr	450	2.0, ~650	70 cycles,100%		[116]
	Ca–Mg||Bi	LiCl–$CaCl_2$	550	0.15, ~50	1400 cycles, 100%		[117]
	Na||Bi–Sn–In	1M NaI in tetraglyme	100	0.1, 1	40 cycles,—	High cost of low melting point metals, SEI evolution at the surface of liquid metal	[118]
	Na–K||Ga–In	1M $NaClO_4$ in DME/FEC(95:5)	25	— ,—	100 cycles, 95%		[119]
	Na–K	1 M KFSI in DME	25	—	100 cycles, 74%		[120]

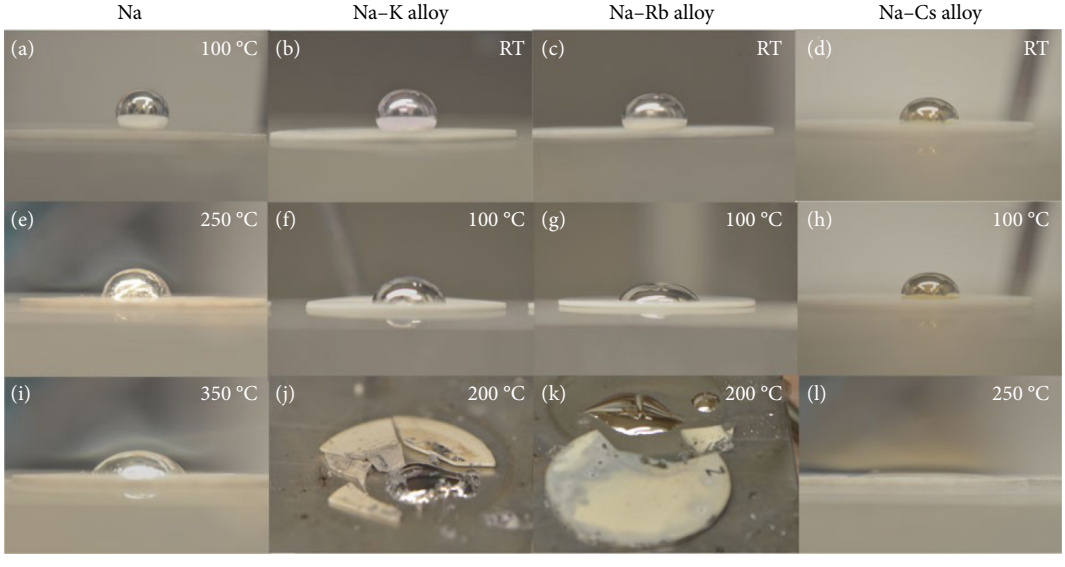

Fig. 9 Wetting behavior of Na and Na–K, Na–Rb, and Na–Cs alloys on the surface of β"Al_2O_3 electrolytes. Reprinted with permission from ref. [106], © 2014 Macmillan Publishers Limited).

al. used magnetron sputtering to coat Sn on the surface of NASICON disks which have higher ionic conductivity than β"-Al_2O_3 electrolytes. The assembled symmetrical battery (Na|NASISON|Na) can operate stably at 110 °C and can withstand the maximum current density of 50 $mA·cm^{-2}$[129]. Subsequently, the Na|Sn coated NASICON|NaI–$GaCl_3$ was constructed and the battery delivers 3.65 V of discharge voltage and outstanding cycling performance (400 cycles)[107].

3.1.3 *Other strategies*

Besides coating and alloying strategies, Jin et al.[108] used liquid metal lithium with strong reducibility (−3.04 V vs. standard hydrogen electrode (S.H.E)) to achieve effective wetting with oxide ceramic electrolytes (garnet-type $Li_{6.4}La_3Zr_{1.4}Ta_{0.6}O_{12}$, LLZTO) and design Li|LLZTO|Pb–X (X = Bi, Sn) batteries at a moderate operating temperature (210–250 °C), as shown in Figure 10. The ionic conductivity of the LLZTO electrolytes was enhanced to 200 times at 240 °C (135 $mS·cm^{-1}$) than that at room temperature (0.7 $mS·cm^{-1}$), which ensures the high rate performance of Li–LLZTO systems[130]. The Li|LLZTO|Pb–Bi battery exhibits three different voltage plateaus of 0.77, 0.58, and 0.4 V during the discharge process, corresponding to the different intermetallic of $Li_{8.5}Bi_3Pb$, $Li_{9.4}Bi_3Pb$, and $Li_{11.5}BiPb$. This battery can deliver ca. 0.8 V discharge voltage and high capacity retention even at 500 $mA·cm^{-2}$, demonstrating the high ionic conductivity of LLZTO electrolytes and the rapid interfacial mass transfer process. Subsequently, semi-liquid cath-

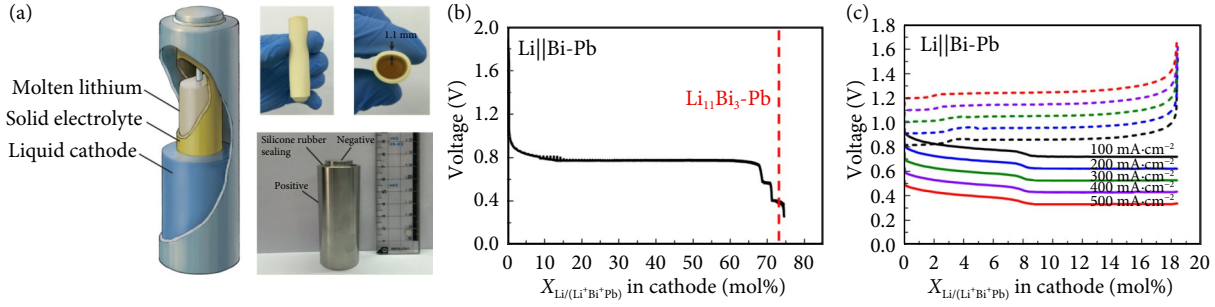

Fig. 10 **(a)** Schematic of the Li|LLZTO|Bi–Pb battery. **(b,c)** Electrochemical performance of Li|LLZTO|Bi–Pb. Reprinted with permission from ref. [108], © The Author(s) 2018.

odes such as Sn–Pb alloy, Bi–Pb alloy[108], sulfur, selenium[130], $AlCl_3$–LiCl[131], Mo–$FeCl_2$[132], Brass–$ZnCl_2$[133] have been reported in liquid Li–LLZTO electrolyte interfaces and demonstrate the good compatibility. These batteries with similar structures to Na–S and ZEBRA battery possess a better interface wettability. However, the operating temperature of them is crucial due to the strong reducibility of liquid lithium metal at high temperature, and the corrosion of oxide ceramic electrolytes should be concerned for developing long-term service Li–LLZTO battery systems.

The above strategies effectively addressed the wettability issue of liquid metal electrodes and improved the performance of the batteries based on liquid metal electrodes-solid electrolytes. However, the preparation of the large-scale solid electrolytes with high quality and high strength still facing challenges, which restricts the practical application of the metal electrode batteries based on liquid metal electrodes-solid electrolytes.

3.2 Liquid–liquid interface construction

A liquid–liquid interface based on liquid electrolytes can effectively solve the wettability issue of the liquid–solid interface. Considering the activity of liquid metal electrodes, only two type electrolytes, molten salt electrolyte, and organic electrolyte can be compatible with liquid metal electrodes. Molten salt electrolytes with good thermal stability can build a stable interface with liquid metals at an enhanced temperature, while organic electrolytes are suitable for metal electrodes with a low melting point (<200 °C). In this section, the significant progress on liquid metal electrode batteries with molten salt electrolytes and organic electrolytes is reviewed.

3.2.1 Liquid metal-molten salt electrolyte interface

The molten salt electrolyte with the advantages of high ionic conductivity, wide voltage window, and great thermal and chemical stability can be an ideal candidate in the liquid metal electrode. Moreover, the liquid–liquid interface can be self-assembled without SEI based on the immiscibility of liquid metal and molten salts, which avoids the performance degradation caused by the decay of the SEI. The typical application of liquid metal–molten salt interface is liquid metal batteries (LMBs), which is proposed by Kim et al. in 2006[134]. LMBs comprises two liquid metal electrodes separated by a molten salt electrolyte that can self-segregate into three-layer.

Antimony (Sb) with low-cost and high electronegativity, is one of the initial reported positive electrodes of LMB. In 2012, Bradwell et al. reported the first LMB in Mg||Sb systems, combined with $MgCl_2$–KCl–NaCl electrolytes[109]. Considering the high melting points of Mg (T_m = 651 °C) and Sb (T_m = 630 °C), the Mg||Sb systems usually operate at a high temperature of 700 °C. The Mg||Sb LMB could deliver ca. 0.5 V electromotive force (EMF), and exhibits about 0.2 V of discharge voltage at 200 mA·cm^{-2}, which verified the feasibility of the liquid–liquid interface based on liquid metal and molten salts for the first time. Subsequently, Wang et al.[110] designed liquid Sb–Pb alloy electrodes and decreased the melting point of Sb-based electrodes from 630 to 250°C. It is reported that, when working at 450 °C, Li||Sb–Pb LMBs based on LiF–LiCl–LiI electrolyte can deliver a 0.75 V discharge voltage at 275 mA·cm^{-2} and 94% capacity retention after 450 cycles, suggesting the excellent cycling stability of liquid metal electrodes (Figures 11(a)–11(c)). Moreover, Li et al.[111] designed Li||Sb–Sn LMBs based on LiF–LiCl–LiBr electrolytes at 500 °C, revealing the dominant role of Sb in the discharge process of Sb–Sn alloy electrodes. The Li||Sb–Sn LMB exhibited 87 % of initial capacity when the current density increased from 0.1 to 1 A·cm^{-2} (Figure 11(d)). In 2021, Yan et al.[112] reported Li||Sb LMBs based on LiF–LiCl–LiBr molten salt electrolyte and solid metal Sb electrode at 500 °C. The Li||Sb system demonstrated a novel conversion process of the solid Sb electrode and liquid Li–Sb alloy during the discharge process(Figures 11(e) and 11(f)), in which the liquid phase of Li–Sb alloy contributed to the self-healing of the electrode structure and ensured the cycling stability of the battery. The Li||Sb system further broadens the design limitations and operating temperature range of LMBs.

Metal bismuth (Bi) with similar electrochemical properties to Sb and a lower melting point (271.5 °C), is a good positive electrode candidate for LMBs. Ning et al. firstly reported the Li||Bi LMB with LiCl–LiF electrolyte, demonstrated the evolution process of the Bi electrode–molten salt electrolyte interface and proved the self-healing properties of liquid metal electrodes (Figure 11(g)). The Li||Bi LMB presented an excellent cyclability of 1000 cycles (Figure 11(h)).[113] The low-melting-point Bi electrode is often used to design low-temperature liquid metal battery systems. For example, the melting point of Bi–Pb eutectic, Bi–Sn alloy, and Wood's alloy (Bi50–Pb25–Sn12.5–Cd12.5 wt%) is 124.5, 141.5, and 70 °C, respectively. Kim et al. used Bi–Pb alloy as the positive electrode to construct Li|LiCl–LiI|Bi–Pb LMB at 410 °C[135]. Yu et al. adopted Bi–Sn alloy and LiI–KI as electrodes and electrolytes and operated the Li|LiI–KI|Bi–Sn LMB at 300 °C[136].

In addition, the construction of a stable liquid–liquid interface also needs to solve the problem of metal dissolution in molten salt electrolytes, such as the dissolution of Na, Ca, and Te electrodes in the corresponding molten salt electrolytes. Although some researchers have been able to effectively inhibit the metal dissolution through alloying strategies, such as Ca–Mg alloy[117] and Te–Sn alloy[116], the long-term service of these battery systems remains challenging. Moreover, the stability of large-size liquid–liquid interfaces and high-temperature sealing of the battery need be further concerned in the development of an LMB for practical applications.

3.2.2 Liquid metal-organic electrolyte interface

The liquid–liquid interface based on low melting point metal and

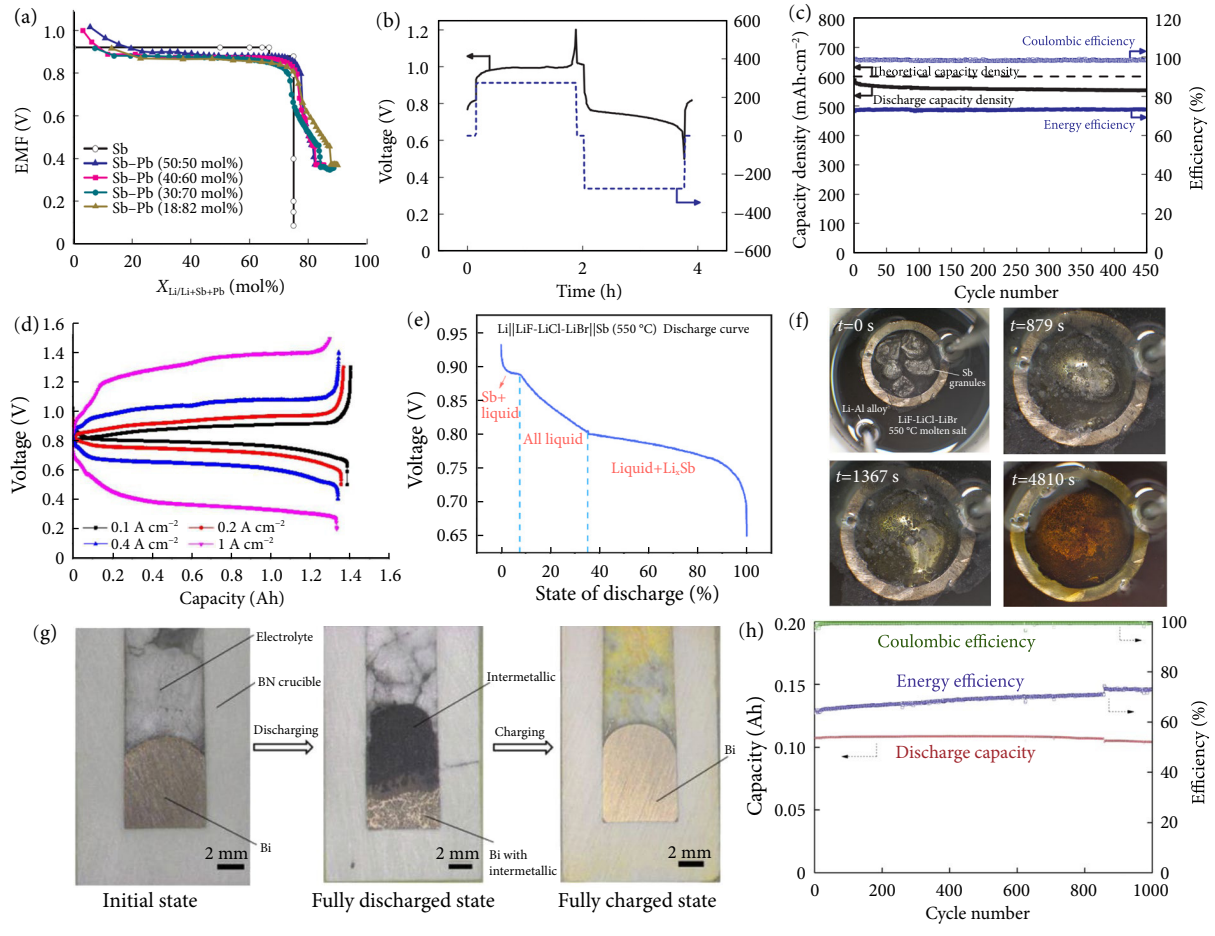

Fig. 11 **(a)** The EMF curves of different Sb–Pb alloys. **(b,c)** The charge-discharge curve and cycle performance of Li||Sb–Pb LMB. (a–c) Reprinted with permission from ref. [110], © 2014 Macmillan Publishers Limited. **(d)** Rate performance of Li||Sb–Sn LMB (reprinted with permission from ref. [111], © 2016 American Chemical Society). **(e,f)** The voltage curves and in-situ observation of the solid–liquid–solid transformation of Sb electrodes during the discharge process. Reprinted with permission from ref. [112], © 2021 Elsevier. **(g)** Cross-sections of Bi electrodes at different depths of discharge. **(h)** Cycling performance of Li|LiCl–LiF|Bi LMB. (g,h) Reprinted with permission from ref. [113], © 2014 Elsevier.

organic electrolytes can avoid a series of problems in high-temperature LMBs. In 2016, Lalau et al. constructed a liquid–liquid interface at 220 °C based on liquid Ga (T_m = 29.8 °C) electrode and 1 M Li[TFSI] in [BMP][TFSI] (1-butyl-1-methylpyrrolidinium bis (trifluoromethylsulfonyl) imide) electrolyte in Li||Ga battery, demonstrating stable operation for 600 h (Figures 12(a) and 12(b))[137]. In 2020, Ding et al.[118] reported Na||Bi–Sn–X (X= In, Pb) LMBs with 1 M NaI (in tetraglyme) electrolyte at 100 °C, and the electrochemical characteristics of different alloys including Bi–Sn–In (62 °C), Bi–Pb–Sn–In (58 °C), or Bi–Pb–Sn (98 °C) were investigated (Figure 12(c)). Figure 12(d) shows the discharge curve of Na||Bi–Sn–In battery, and the capacity retention of this cell after 40 cycles is nearly 100% (Figure 12(e)). Further, Ding et al.[119] used Na–K alloy as the negative electrode, 1 M $NaClO_4$ in the DME/FEC (95:5 vol%) as the electrolyte, and Ga–In (or Ga–Sn) alloy as the positive electrode to construct the first Na–K||Ga–In LMB at room temperature. The Na–K||Ga–In batteries delivered a discharging voltage of 0.5 V at 100 mA·g^{-1}, and good cycling performance (without capacity fading after 100 cycles), suggesting the excellent stability of the liquid metal interface. However, the ionic conductivity of the organic electrolyte is 2–3 orders of magnitude lower than that of molten salt electrolytes, which limits the power density of the room temperature LMBs. Moreover, similar to the solid metal electrode batteries, liquid metal electrodes with high reducibility will inevitably react with the organic electrolyte to form SEI, which will lead to an irreversible capacity loss of liquid electrodes. This interaction has been proved in the Li||Ga battery, in which the volume changes of the liquid Ga electrode induced the SEI evolution, leading to a large (75%) irreversible capacity loss in the first few cycles[125].

Above all, the liquid–liquid interface based on liquid metal electrodes and molten salts/organic electrolytes demonstrate the excellent cycling stability in LMBs. Nevertheless, there are still some issues hindering the application of LMBs, including high temperatures in molten salt electrolyte batteries and instability of the SEI in organic electrolyte batteries. Therefore, the LMBs at an intermediate operated temperature (100–300 °C) based on low melting point molten salts or ionic liquid electrolytes should be an important direction of the development of batteries based on liquid–liquid interface.

3.3 Interfacial chemical stability

The interfacial chemical instability in liquid metal batteries mainly results from the side reactions between liquid metal electrodes and battery parts, such as metal current collectors, insulators, and shells, at a high operating temperature. On the one hand, these side reactions will consume the liquid metal electrodes, resulting in the capacity fading of the battery. On the other hand, severe

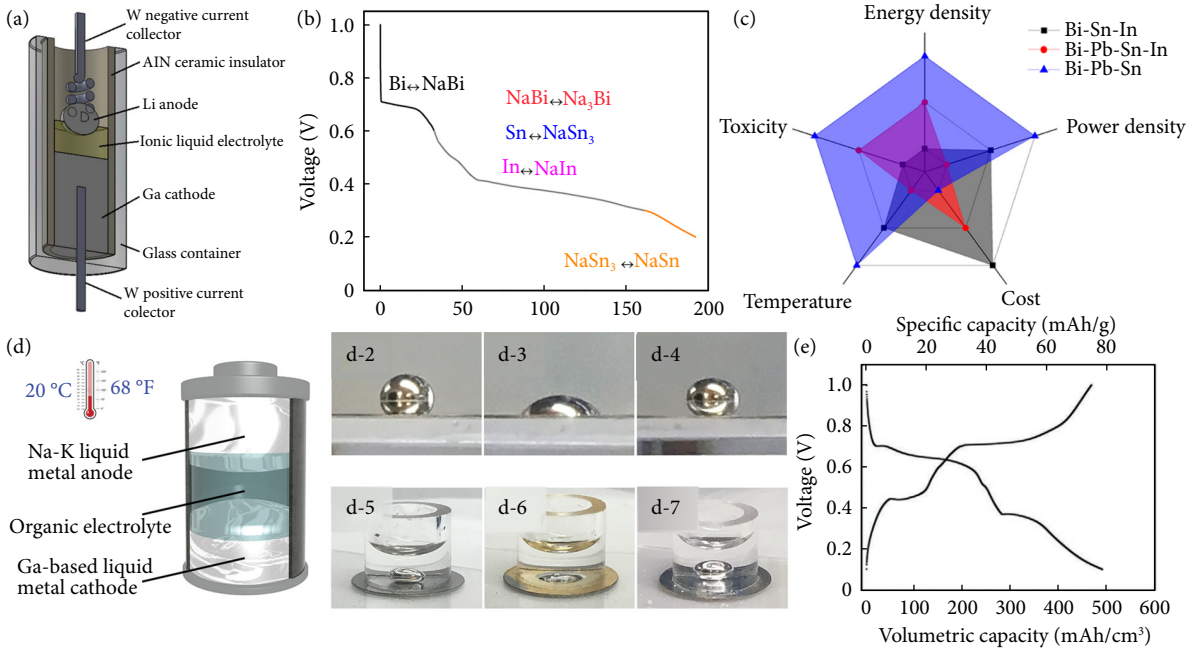

Fig. 12 **(a)** The configuration and discharge curves of Li||Ga LMB (10 mA cm-2). **(b)** Dischage profile of Bi–In–Sn vs Na at a specific current of 80 mA/g. (a,b) Reprinted with permission from ref. [137], © 2016 The Electrochemical Society. **(c)** The comparison of some low melting point liquid metal electrodes. Reprinted with permission from ref. [118], © 2020 American Chemical Society. **(d-1)** Configuration of the room temperature Na–K||Ga–In LMB. The wettability test of Ga–In alloys on the surface of different substrates in the air or Na electrolyte: stainless steel **(d-2, d-5)**, Au-coated stainless steel **(d-3,d-6)**, and Al-coated stainless steel **(d-4,d-7)**. **(e)** The charge-discharge curve of the Na–K||Ga–In LMB. (d,e) Reprinted with permission from ref. [119], © 2020 Wiley-VCH.

corrosion of battery components, especially ceramic insulators, will cause battery leakage and thereby leading to complete battery failure.

3.3.1 *Corrosion of current collectors*

Corrosion of the current collector in liquid metal electrodes usually occurs at high operating temperatures (>300 °C), especially for LMBs. Generally, the negative electrodes of LMBs are Li, Na, Ca, Mg, and the positive electrodes are liquid Bi, Sb, Sn, Pb, and their alloys. The current collectors of LMBs are Fe-based alloys including the elements of Fe, Ni, Cr, Mn, and C, etc. Taking the metal Li as an example, the corrosion mechanism of Li is mainly physical dissolution and chemical corrosion. Many researches have investigated the corrosion behaviors of liquid lithium metal on stainless steel and verified the effect of impurities and temperature have on the corrosion rate of it[138,139].

Compared with the corrosion of anodes, the corrosion of the cathode collector is more serious. Cui et al.[140] investigated the static and dynamic corrosion process of SS304 current collector by liquid Sb–Sn alloy in Li||Sb–Sn LMBs at 500 °C, demonstrating the Fe and Cr in 304ss are more easily corroded by Sb–Sn alloys (Figure 13(a)). The corrosion products of Fe–Ni–Sb–Sn will decrease the discharge voltage of the Li||Sb–Sn LMBs, accelerating the capacity fading process. The metal Sn in Sb–Sn alloy electrodes can promote the ions diffusion and accelerate the corrosion of the current collector. Ouchi et al.[141] ademonstrated a comparative study for the corrosion behavior of low carbon steel, 301 stainless steel (SS301) and 430 stainless steel (SS430), in liquid Pb–Sb alloy at 450 °C. The results showed that Sb in Pb–Sb alloy reacted with Fe, Cr, and Ni in stainless steel to form intermetallic compounds. Compared with the stainless steel SS430 containing Cr, the corrosion resistance of SS301 containing Ni is weaker (Figure 13(b)). Moreover, the authors further investigated the corrosion behavior of metal Mo, Ti, and W in liquid Sb–Sn alloy electrodes (Figure 13(c))[142], demonstrated the good corrosion resistance of metal W, which guides the selection of liquid metal battery collector.

3.3.2 *Corrosion of sealing*

In general, liquid metal electrodes are highly sensitive to water and oxygen and the side reactions with them will cause serious side reactions, resulting in capacity fading and even safety issues. A good sealing design can avoid side reactions and ensure the long-term cycling of the battery. Because the conventional organic sealing are difficult to meet the sealing requirements at the high temperature above 200 °C, seals of liquid metal based batteries generally choose ceramic materials. For example, Na–S batteries and ZEBRA batteries generally adopt the hot-pressing sealing technology of Al–Al_2O_3–Al sandwich structure[143], which is formed by exposing the aluminum layer on alumina substrate to high pressure and heat to promote interatomic diffusion. However, the Al_2O_3-based sealing is not suitable for lithium-based liquid metal batteries for the liquid lithium metal can reduce Al_2O_3. In terms of high-temperature stability and insulation, nitride ceramics are an ideal choice, and aluminum nitride (AlN) ceramics are considered as one of the potential candidates for battery insulators. Nagura et al. and Terai et al. [144,145] demonstrated the corrosion resistance of AlN in liquid Li metal at 400 and 500 °C. Although nitride ceramics are resistant to corrosion from liquid lithium metal at high temperature, welding ceramics to metal is still a huge challenge. Therefore, the long-term sealing of the battery at high temperature is still plaguing for the development of high temperature LMBs.

4 Conclusions and outlook

Interfacial engineering is critical for addressing the interface issues including dendrite, the evolution of SEI and instability of metal electrodes to achieve the next-generation energy storage batteries

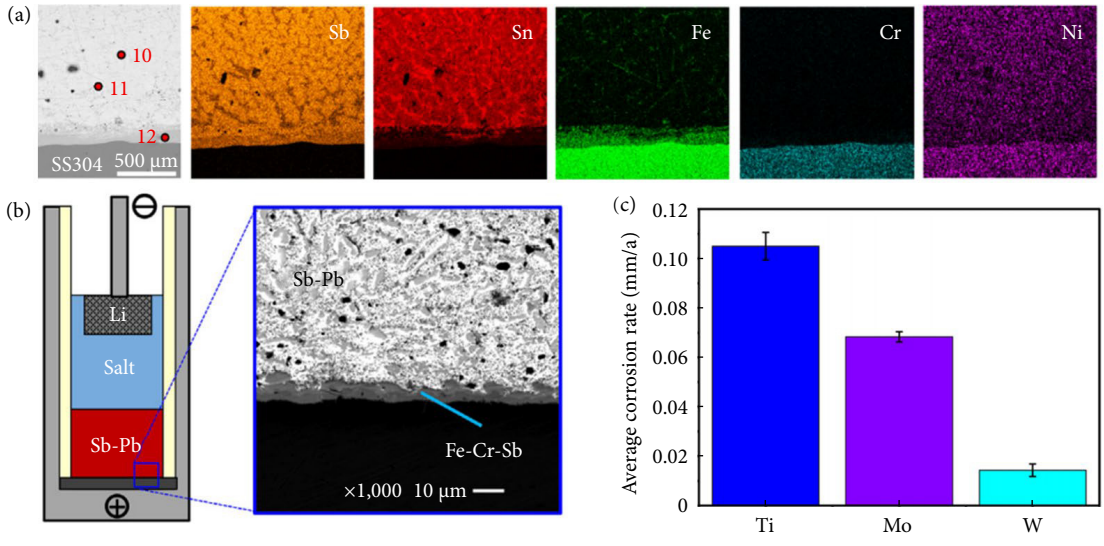

Fig. 13 **(a)** Cross-sectional SEM images and EDS element mapping images about corrosion of SS304 in Sb–Sn alloy at 500 °C for 500 h (reprinted with permission from ref. [140], © 2021 American Chemical Society). **(b)** The corrosion results of SS430 in Pb–Sb alloy at 450 °C for 500 h (reprinted with permission from ref. [141], © 2017 Elsevier). **(c)** The corrosion rate of metal Ti, Mo and W in liquid Sb–Sn alloys at 500 °C (reprinted with permission from ref. [142], © 2021 American Chemical Society).

with high specific energy and long lifespan. In this review, the interface issues of metal electrode are systematically analyzed, the dendrite growth mechanisms and SEI evolution laws of metal electrodes are demonstrated, and the influencing factors of interface stability of metal electrode are demonstrated. Then, the interfacial engineering efforts on metal electrode are summarized in different categories, including the intrinsic transport dynamics optimization, interfacial chemistry regulation and solid–solid interface construction. Moreover, a potential alternative for metal electrode batteries, liquid metal electrode batteries, are reviewed. Similarly, the interfacial problems have been proposed and some strategies have been introduced. For instance, the enhancement of the liquid metal electrodes wettability, the construction of the liquid–liquid interface and the measurement of the chemical stable interface.

Although numerous progresses in metal electrode interface engineering have been achieved, the practical application of metal electrode batteries is still challenging. In terms of the whole battery, the side reactions derived from the metal electrode modification, such as 3D collector design, still need to be further solved. The utilization ratio of metal electrodes, CE and long-term stability of metal electrode batteries should be still concerned. Moreover, the design of electrolyte additives for practical application still needs to be optimized, and the cost control of some lithium salt and solvent is of great significant for a practical battery system, which should be raised enough attention. Furthermore, innovative battery architecture design, for instance all-solid-state batteries and liquid metal batteries, is an important way to solve the interface issues of metal electrodes. All-solid-state batteries based on the SSEs can suppress the dendrite formation of the metal electrode, should be one of most promising choice for high specific energy storage application. Moreover, the design of liquid metal electrode broadens a new way for the development of metal electrode batteries, fundamentally getting rid of many interface issues of solid metal electrodes. And the LMBs based on liquid metal electrodes are considered as an ideal choice for the large-scale energy storage applications. However, the interface issues of high contact resistance in all-solid-state batteries and high temperature sealing and corrosion in liquid metal batteries still need to be further addressed before the practical application.

Acknowledgements

This work is supported by National Key Research and Development Program of China (2018YFB0905600), and grants from the National Natural Science Foundation of China (Grant Nos. 52177215, 51977097, 51861135315, 51804128).

Article history

Received: 6 June 2022; Revised: 27 June 2022; Accepted: 17 July 2022

Additional information

Declaration of competing interest

The authors have no competing interests to declare that are relevant to the content of this article.

References

[1] Ma, L., Cui, J., Yao, S., Liu, X., Luo, Y., Shen, X., Kim, J. K. (2022). Dendrite-free lithium metal and sodium metal batteries. *Energy Storage Materials*, 27: 522–554.

[2] Laszczynski, S. V., Gorski, S. V. (1897). Leitfähigkeit von Lösungen Eniger Saltze in Pyridin. *Z. Elektrochem*, 4: 290–293.

[3] Li, C. P., Xie, X. S., Liang, S. Q., Zhou, J. (2020). Issues and future perspective on zinc metal anode for rechargeable aqueous zinc-ion batteries. *Energy & Environmental Materials*, 3: 146–159.

[4] Gao, X. W., Zhou, Y. N., Han, D. Z., Zhou, J. Q., Zhou, D. Z., Tang, W., Goodenough, J. B. (2020). Thermodynamic understanding of Li-dendrite formation. *Joule*, 4: 1864–1879.

[5] Gao, M. D., Li, H., Xu, L., Xue, Q., Wang, X. R., Bai, Y., Wu, C. (2021). Lithium metal batteries for high energy density: Fundamental electrochemistry and challenges. *Journal of Energy Chemistry*, 59: 666–687.

[6] Chazalviel, J. (1990). Electrochemical aspects of the generation of

ramified metallic electrodeposits. *Physical Review A*, 42: 7355–7367.
[7] Ely, D., García, R. E. (2013). Heterogeneous nucleation and growth of lithium electrodeposits on negative electrodes. *Journal of the Electrochemical Society*, 160: A662–A668.
[8] Brissot, C., Rosso, M., Chazalviel, J. N., Lascaud, S. (1999). Dendritic growth mechanisms in lithium/polymer cells. *Journal of Power Sources,* 81–82: 925–929.
[9] Guyer, J. E., Boettinger, W. J., Warren, J. A., McFadden, G. B. (2004). Phase field modeling of electrochemistry. I. Equilibrium. *Physical Review E*, 69: 021603.
[10] Dey, A. N., Sullivan, B. P. (1970). The electrochemical decomposition of propylene carbonate on graphite. *Journal of the Electrochemical Society,* 117: 222.
[11] Peled, E. (1979). The electrochemical behavior of alkali and alkaline earth metals in nonaqueous battery systems—The solid electrolyte interphase model. *Journal of the Electrochemical Society*, 126: 2047–2051.
[12] Cheng, X. B., Zhang, R., Zhao, C. Z., Zhang, Q. (2017). Toward safe lithium metal anode in rechargeable batteries: A review. *Chemical Reviews*, 117: 10403–10473.
[13] Vogt, L. O., El Kazzi, M., Jämstorp Berg, E., Pérez Villar, S., Novák, P., Villevieille, C. (2015). Understanding the interaction of the carbonates and binder in Na-ion batteries: A combined bulk and surface study. *Chemistry of Materials*, 27: 1210–1216.
[14] Men, S., Zheng, H., Ma, D. J., Huang, X. L., Kang, X. W. (2021). Unraveling the stabilization mechanism of solid electrolyte interface on ZnSe by rGO in sodium ion battery. *Journal of Energy Chemistry*, 54: 124–130.
[15] Huang, J., Guo, X., Du, X., Lin, X., Huang, J. Q., Tan, H. Zhu, Y., Zhang, B. (2019). Nanostructures of solid electrolyte interphases and their consequences for microsized Sn anodes in sodium ion batteries. *Energy & Environmental Science*, 12: 1550–1557.
[16] Wang, Z. H., Yang, H. Y., Liu, Y. R., Bai, Y., Chen, G. H., Li, Y., Wang, X. R., Xu, H. J., Wu, C., Lu, J. (2020). Analysis of the stable interphase responsible for the excellent electrochemical performance of graphite electrodes in sodium-ion batteries. *Small*, 16: 2003268.
[17] Shi, S. Q., Lu, P., Liu, Z. Y., Qi, Y., Hector, L. G. Jr, Li, H., Harris, S. J. (2012). Direct calculation of Li-ion transport in the solid electrolyte interphase. *Journal of the American Chemical Society*, 134: 15476–15487.
[18] Kim, S. P., van Duin, A. C. T., Shenoy, V. B. (2011). Effect of electrolytes on the structure and evolution of the solid electrolyte interphase (SEI) in Li-ion batteries: A molecular dynamics study. *Journal of Power Sources*, 196: 8590–8597.
[19] Shi, Y., Liu, G. X., Wan, J., Wen, R., Wan, L. J. (2021). In-situ nanoscale insights into the evolution of solid electrolyte interphase shells: Revealing interfacial degradation in lithium metal batteries. *Science China Chemistry*, 64: 734–738.
[20] Kinzer, B., Davis, A. L., Krauskopf, T., Hartmann, H., LePage, W. S., Kazyak, E., Janek, J., Dasgupta, N. P., Sakamoto, J. (2021). Operando analysis of the molten Li|LLZO interface: Understanding how the physical properties of Li affect the critical current density. *Matter*, 4: 1947–1961.
[21] Tantratian, K., Yan, H. H., Ellwood, K., Harrison, E. T., Chen, L. (2021). Unraveling the Li penetration mechanism in polycrystalline solid electrolytes. *Advanced Energy Materials*, 11: 2003417.
[22] Kim, S., Kim, J. S., Miara, L., Wang, Y., Jung, S. K., Park, S. Y., Song, Z., Kim, H., Badding, M., Chang, J., et al. (2022). High-energy and durable lithium metal batteries using garnet-type solid electrolytes with tailored lithium-metal compatibility. *Nature Communications*, 13: 1883.
[23] Beverskog, B., Puigdomenech, I. (1997). Revised pourbaix diagrams for zinc at 25–300 °C. *Corrosion Science*, 39: 107–114.
[24] Lukatskaya, M. R., Dunn, B., Gogotsi, Y. (2016). Multidimensional materials and device architectures for future hybrid energy storage. *Nature Communications*, 7: 12647.
[25] Yue, Y., Liang, H. (2018). 3D current collectors for lithium-ion batteries: A topical review. *Small Methods*, 2: 1800056.
[26] Liu, S., Tang, S., Zhang, X. Y., Wang, A. X., Yang, Q. H., Luo, J. Y. (2017). Porous Al current collector for dendrite-free Na metal anodes. *Nano Letters*, 17: 5862–5868.
[27] Sim, W. H., Jeong, H. M. (2021). Efficient lithium growth control from ordered nitrogen-chelated lithium-ion for high performance lithium metal batteries. *Advanced Science*, 8: 2002144.
[28] Zhang, R., Wen, S. W., Wang, N., Qin, K. Q., Liu, E. Z., Shi, C. S., Zhao, N. Q. (2018). N-doped graphene modified 3D porous Cu current collector toward microscale homogeneous Li deposition for Li metal anodes. *Advanced Energy Materials*, 8: 1800914.
[29] Sun, J. C., Guo, C. P., Cai, Y. J., Li, J. J., Sun, X. Q., Shi, W. J., Ai, S. Y., Chen, C. C., Jiang, F. Y. (2019). Dendrite-free and long-life Na metal anode achieved by 3D porous Cu. *Electrochimica Acta*, 309: 18–24.
[30] Pan, L. H., Luo, Z. F., Zhang, Y. T., Chen, W. L., Zhao, Z. H., Li, Y. Y., Wan, J., Yu, D. D., He, H. Y., Wang, D. Y. (2019). Seed-free selective deposition of lithium metal into tough graphene framework for stable lithium metal anode. *ACS Applied Materials & Interfaces*, 11: 44383–44389.
[31] Jin, D., Park, J., Ryou, M. H., Lee, Y. M. (2020). Structure-controlled Li metal electrodes for post-Li-ion batteries: Recent progress and perspectives. *Advanced Materials Interfaces*, 7: 1902113.
[32] Chen, K. H., Sanchez, A. J., Kazyak, E., Davis, A. L., Dasgupta, N. P. (2019). Synergistic effect of 3D current collectors and ALD surface modification for high coulombic efficiency lithium metal anodes. *Advanced Energy Materials*, 9: 1802534.
[33] Wu, S. L., Jiao, T. P., Yang, S. R., Liu, B., Zhang, W. J., Zhang, K. L. (2019). Lithiophilicity conversion of the Cu surface through facile thermal oxidation: Boosting a stable Li–Cu composite anode through melt infusion. *Journal of Materials Chemistry A*, 7: 5726–5732.
[34] Huang, X., Feng, X. Y., Zhang, B., Zhang, L., Zhang, S. C., Gao, B., Chu, P. K., Huo, K. F. (2019). Lithiated $NiCo_2O_4$ nanorods anchored on 3D nickel foam enable homogeneous Li plating/stripping for high-power dendrite-free lithium metal anode. *ACS Applied Materials & Interfaces*, 11: 31824–31831.
[35] Lin, H. N., Zhang, Z. W., Wang, Y. D., Zhang, X. L., Tie, Z. X., Jin, Z. (2021). Template-sacrificed hot fusion construction and nanoseed modification of 3D porous copper nanoscaffold host for stable-cycling lithium metal anodes. *Advanced Functional Materials*, 31: 2102735.
[36] Li, J., Zou, P. C., Chiang, S. W., Yao, W. T., Wang, Y., Liu, P., Liang, C. W., Kang, F. Y., Yang, C. (2020). A conductive-dielectric gradient framework for stable lithium metal anode. *Energy Storage Materials*, 24: 700–706.
[37] Wang, C. L., Wang, H., Matios, E., Hu, X. F., Li, W. Y. (2018). A chemically engineered porous copper matrix with cylindrical core–shell skeleton as a stable host for metallic sodium anodes. *Advanced Functional Materials*, 28: 1802282.
[38] Guo, W. B., Cong, Z. F., Guo, Z. H., Chang, C. Y., Liang, X. Q., Liu, Y. D., Hu, W. G., Pu, X. (2020). Dendrite-free Zn anode with dual channel 3D porous frameworks for rechargeable Zn batteries. *Energy Storage Materials*, 30: 104–112.
[39] Fan, X. Y., Yang, H., Wang, X. X., Han, J. X., Wu, Y., Gou, L., Li, D. L., Ding, Y. L. (2021). Enabling stable Zn anode via a facile alloying strategy and 3D foam structure. *Advanced Materials Interfaces*, 8: 2002184.
[40] Liu, L, Yin, Y. X., Li, J. Y., Wang, S. H., Guo, Y. G., Wan, L. J. (2018). Uniform lithium nucleation/growth induced by lightweight nitrogen-doped graphitic carbon foams for high-performance lithium metal anodes. *Advanced Materials*, 30: 1706216.

[41] Wang, T. S., Liu, X. B., Wang, Y., Fan, L. Z. (2021). High areal capacity dendrite-free Li anode enabled by metal–organic framework-derived nanorod array modified carbon cloth for solid state Li metal batteries. *Advanced Functional Materials*, 31: 2001973.

[42] Li, T. J., Sun, J. C., Gao, S. Z., Xiao, B., Cheng, J. B., Zhou, Y. L., Sun, X. Q., Jiang, F. Y., Yan, Z. H., Xiong, S. L. (2021). Superior sodium metal anodes enabled by sodiophilic carbonized coconut framework with 3D tubular structure. *Advanced Energy Materials*, 11: 2003699.

[43] Chi, S. S., Qi, X. G., Hu, Y. S., Fan, L. Z. (2018). 3D flexible carbon felt host for highly stable sodium metal anodes. *Advanced Energy Materials*, 8: 1702764.

[44] Zeng, Y. X., Zhang, X. Y., Qin, R. F., Liu, X. Q., Fang, P. P., Zheng, D. Z., Tong, Y. X., Lu, X. H. (2019). Dendrite-free zinc deposition induced by multifunctional CNT frameworks for stable flexible Zn-ion batteries. *Advanced Materials*, 31: e1903675.

[45] Xue, P., Guo, C., Wang, N., Zhu, K., Jing, S., Kong, S., Zhang, X., Li, L., Li, H., Feng, Y., et al. (2021). Synergistic manipulation of Zn^{2+} ion flux and nucleation induction effect enabled by 3D hollow SiO_2/TiO_2/carbon fiber for long-lifespan and dendrite-free Zn-metal composite anodes. *Advanced Functional Materials*, 31: 2106417.

[46] Gu, Y., Xu, H. Y., Zhang, X. G., Wang, W. W., He, J. W., Tang, S., Yan, J. W., Wu, D. Y., Zheng, M. S., Dong, Q. F., et al. (2019). Lithiophilic faceted Cu (100) surfaces: High utilization of host surface and cavities for lithium metal anodes. *Angewandte Chemie International Edition*, 58: 3092–3096.

[47] Zheng, J. X., Zhao, Q., Tang, T., Yin, J. F., Quilty, C. D., Renderos, G. D., Liu, X., Deng, Y., Wang, L., Bock, D. C., et al. (2019). Reversible epitaxial electrodeposition of metals in battery anodes. *Science*, 366: 645–648.

[48] Zhang, Y., Han, X., Liu, R., Yang, Z., Zhang, S., Zhang, Y., Wang, H., Cao, Y., Chen, A., Sun, J. (2022). Manipulating the Zinc deposition behavior in hexagonal patterns at the preferential Zn (100) crystal plane to construct surficial dendrite-free zinc metal anode. *Small*, 18: 2105978.

[49] Liang, X., Pang, Q., Kochetkov, I. R., Sempere, M. S., Huang, H., Sun, X. Q., Nazar, L. F. (2017). A facile surface chemistry route to a stabilized lithium metal anode. *Nature Energy*, 2: 17119.

[50] Baggetto, L., Keum, J. K., Browning, J. F., Veith, G. M. (2013). Germanium as negative electrode material for sodium-ion batteries. *Electrochemistry Communications*, 34: 41–44.

[51] Liu, B. T., Wang, S. J., Wang, Z. L., Lei, H., Chen, Z. T., Mai, W. J. (2020). Novel 3D nanoporous Zn-Cu alloy as long-life anode toward high-voltage double electrolyte aqueous zinc-ion batteries. *Small*, 16: e2001323.

[52] Ye, H., Zheng, Z. J., Yao, H. R., Liu, S. C., Zuo, T. T., Wu, X. W., Yin, Y. X., Li, N. W., Gu, J. J., Cao, F. F., et al. (2019). Guiding uniform Li plating/stripping through lithium–aluminum alloying medium for long-life Li metal batteries. *Angewandte Chemie*, 131: 1106–1111.

[53] Sultana, I., Rahman, M. M., Chen, Y., Glushenkov, A. M. (2018). Potassium-ion battery anode materials operating through the alloying –dealloying reaction mechanism. *Advanced Functional Materials*, 28: 1703857.

[54] von Aspern, N., Röschenthaler, G. V., Winter, M., Cekic–Laskovic, I. (2019). Fluor und lithium: Ideale partner für elektrolyte in wiederaufladbaren hochleistungsbatterien. *Angewandte Chemie*, 131: 16124–16147.

[55] Zhang, X. Q., Cheng, X. B., Chen, X., Yan, C., Zhang, Q. (2017). Fluoroethylene carbonate additives to render uniform Li deposits in lithium metal batteries. *Advanced Functional Materials*, 27: 1605989.

[56] Yu, Z. A., Wang, H. S., Kong, X., Huang, W., Tsao, Y., Mackanic, D. G., Wang, K. C., Wang, X. C., Huang, W. X., Choudhury, S., et al. (2020). Molecular design for electrolyte solvents enabling energy-dense and long-cycling lithium metal batteries. *Nature Energy*, 5: 526–533.

[57] Wang, H. S., Yu, Z. A., Kong, X., Huang, W., Zhang, Z. W., Mackanic, D. G., Huang, X. Y., Qin, J., Bao, Z. N., Cui, Y. (2021). Dual-solvent Li-ion solvation enables high-performance Li-metal batteries. *Advanced Materials*, 33: e2008619.

[58] Lin, D. C., Liu, Y. Y., Cui, Y. (2017). Reviving the lithium metal anode for high-energy batteries. *Nature Nanotechnology*, 12: 194–206.

[59] Yamada, Y., Furukawa, K., Sodeyama, K., Kikuchi, K., Yaegashi, M., Tateyama, Y., Yamada, A. (2014). Unusual stability of acetonitrile-based superconcentrated electrolytes for fast-charging lithium-ion batteries. *Journal of the American Chemical Society*, 136: 5039–5046.

[60] Lu, H., Zhu, Y., Yuan, Y., He, L., Zheng, B., Zheng, X. Z., Liu, C. C., Du, H. L. (2021). LiFSI as a functional additive of the fluorinated electrolyte for rechargeable Li-S batteries. *Journal of Materials Science: Materials in Electronics*, 32: 5898–5906.

[61] Li, X., Zheng, J. M., Engelhard, M. H., Mei, D. H., Li, Q. Y., Jiao, S. H., Liu, N., Zhao, W. G., Zhang, J. G., Xu, W. (2018). Effects of imide–orthoborate dual-salt mixtures in organic carbonate electrolytes on the stability of lithium metal batteries. *ACS Applied Materials & Interfaces*, 10: 2469–2479.

[62] Xiang, H. F., Shi, P. C., Bhattacharya, P., Chen, X. L., Mei, D. H., Bowden, M. E., Zheng, J. M., Zhang, J. G., Xu, W. (2016). Enhanced charging capability of lithium metal batteries based on lithium bis(trifluoromethanesulfonyl)imide-lithium bis(oxalato) borate dual-salt electrolytes. *Journal of Power Sources*, 318: 170–177.

[63] Brown, Z., Lucht, B. (2018). Synergistic performance of lithium difluoro(oxalato)borate and fluoroethylene carbonate in carbonate electrolytes for lithium metal anodes. *Journal of The Electrochemical Society*, 166: A5117.

[64] Judez, X., Zhang, H., Li, C., González-Marcos, J. A., Zhou, Z., Armand, M., Rodriguez-Martinez, L. M. (2017). Lithium bis (fluorosulfonyl) imide/poly (ethylene oxide) polymer electrolyte for all solid-state Li–S cell. *The Journal of Physical Chemistry Letters*, 8: 1956–1960.

[65] Hilder, M., Howlett, P. C., Saurel, D., Gonzalo, E., Basile, A., Armand, M., Rojo, T., Kar, M., MacFarlane, D. R., Forsyth, M. (2018). The effect of cation chemistry on physicochemical behaviour of superconcentrated NaFSI based ionic liquid electrolytes and the implications for Na battery performance. *Electrochimica Acta*, 268: 94–100.

[66] Kim, H. J., Voronina, N., Yashiro, H., Myung, S. T. (2020). High-voltage stability in KFSI nonaqueous carbonate solutions for potassium-ion batteries: Current collectors and coin-cell components. *ACS Applied Materials & Interfaces*, 12: 42723–42733.

[67] Zheng, Y., Soto, F. A., Ponce, V., Seminario, J. M., Cao, X., Zhang, J. G., Balbuena, P. B. (2019). Localized high concentration electrolyte behavior near a lithium–metal anode surface. *Journal of Materials Chemistry A*, 7: 25047–25055.

[68] Geng, C. X., Buchholz, D., Kim, G. T., Carvalho, D. V., Zhang, H., Chagas, L. G., Passerini, S. (2019). Influence of salt concentration on the properties of sodium-based electrolytes. *Small Methods*, 3: 1800208.

[69] Zhang, Y., Zuo, T. T., Popovic, J., Lim, K., Yin, Y. X., Maier, J., Guo, Y. G. (2020). Towards better Li metal anodes: Challenges and strategies. *Materials Today*, 33: 56–74.

[70] Wang, Y. L., Duan, J. L., Duan, Y. Y., Zhao, Y. Y., Pang, Z. B., He, B. L., Tang, Q. W. (2017). Interfacial engineering of hybridized solar cells for simultaneously harvesting solar and rain energies. *Journal of Materials Chemistry A*, 5: 18551–18560.

[71] Li, J. Q., Yang, Y., Wang, J., Zhang, P., Zhao, J. B. (2017). Elec-

trophoretic deposition of MnO_x@Carbon nanotubes film with nest-like structure as high-performance anode for lithium-ion batteries. *ChemElectroChem*, 4: 679–685.

[72] Wang, M. M., Wang, P., Li, C. P., Li, H. J., Jin, Y. D. (2018). Boosting electrocatalytic oxygen evolution performance of ultrathin Co/Ni-MOF nanosheets via plasmon-induced hot carriers. *ACS Applied Materials & Interfaces*, 10: 37095–37102.

[73] Zhao, Y., Goncharova, L. V., Lushington, A., Sun, Q., Yadegari, H., Wang, B., Xiao, W., Li, R., Sun, X. (2017). Superior stable and long life sodium metal anodes achieved by atomic layer deposition. *Advanced Materials*, 29: 1606663.

[74] Zhao, K. N., Wang, C. X., Yu, Y. H., Yan, M. Y., Wei, Q. L., He, P., Dong, Y. F., Zhang, Z. Y., Wang, X. D., Mai, L. Q. (2018). Ultrathin surface coating enables stabilized zinc metal anode. *Advanced Materials Interfaces*, 5: 1800848.

[75] Hu, J. M., Ding, J., Zhong , Q. (2020). In situ fabrication of amorphous TiO_2/NH_2-MIL-125(Ti) for enhanced photocatalytic CO_2 into CH_4 with H_2O under visible-light irradiation. *Journal of Colloid and Interface Science*, 560: 857–865.

[76] Gao, Y., Yan, Z. F., Gray, J. L., He, X., Wang, D. W., Chen, T. H., Huang, Q. Q., Li, Y. C., Wang, H. Y., Kim, S. H., et al. (2019). Polymer–inorganic solid–electrolyte interphase for stable lithium metal batteries under lean electrolyte conditions. *Nature Materials*, 18: 384–389.

[77] Zhang, H. M., Liao, X. B., Guan, Y. P., Xiang, Y., Li, M., Zhang, W. F., Zhu, X. Y., Ming, H., Lu, L., Qiu, J. Y., et al. (2018). Lithiophilic-lithiophobic gradient interfacial layer for a highly stable lithium metal anode. *Nature Communications*, 9: 3729.

[78] Li, P. L., Dong, X. L., Li, C., Liu, J. Y., Liu, Y., Feng, W. L., Wang, C. X., Wang, Y. G., Xia, Y. Y. (2019). Anchoring an artificial solid–electrolyte interphase layer on a 3D current collector for high-performance lithium anodes. *Angewandte Chemie International Edition*, 58: 2093–2097.

[79] Chi, X. W., Hao, F., Zhang, J. B., Wu, X. W., Zhang, Y., Gheytani, S., Wen, Z. Y., Yao, Y. (2019). A high-energy quinone-based all-solid-state sodium metal battery. *Nano Energy*, 62: 718–724.

[80] Choudhury, S., Wei, S. Y., Ozhabes, Y., Gunceler, D., Zachman, M. J., Tu, Z. Y., Shin, J. H., Nath, P., Agrawal, A., Kourkoutis, L. F., et al. (2017). Designing solid-liquid interphases for sodium batteries. *Nature Communications*, 8: 898.

[81] Tang, X., Zhou, D., Li, P., Guo, X., Sun, B., Liu, H., Yan, K., Gogotsi, Y., Wang, G. X. (2020). MXene-based dendrite-free potassium metal batteries. *Advanced Materials*, 32: e1906739.

[82] Liu, P. C., Wang, Y. X., Gu, Q. L., Nanda, J., Watt, J., Mitlin, D. (2020). Dendrite-free potassium metal anodes in a carbonate electrolyte. *Advanced Materials*, 32: e1906735.

[83] Yang, Q., Ding, Y., He, G. (2020). An amalgam route to stabilize potassium metal anodes over a wide temperature range. *Chemical Communications*, 56: 3512–3515.

[84] Liu, M. K., Cai, J. Y., Ao, H. S., Hou, Z. G., Zhu, Y. C., Qian, Y. T. (2020). $NaTi_2(PO_4)_3$ solid-state electrolyte protection layer on Zn metal anode for superior long-life aqueous zinc-ion batteries. *Advanced Functional Materials*, 30: 2004885.

[85] Zhao, Y., Goncharova, L. V., Zhang, Q., Kaghazchi, P., Sun, Q., Lushington, A., Wang, B. Q., Li, R. Y., Sun, X. L. (2017). Inorganic –organic coating via molecular layer deposition enables long life sodium metal anode. *Nano Letters*, 17: 5653–5659.

[86] Zou, K. Y., Cai, P., Deng, X. L., Wang, B. W., Liu, C., Luo, Z., Lou, X. M., Hou, H. S., Zou, G. Q., Ji, X. B. (2021). Correction: Highly stable zinc metal anode enabled by oxygen functional groups for advanced Zn-ion supercapacitors. *Chemical Communications*, 57: 2571–2572.

[87] Cai, M. L., Lu, Y., Su, J. M., Ruan, Y. D., Chen, C. H., Chowdari, B. V. R., Wen, Z. Y. (2019). In situ lithiophilic layer from H^+/Li^+ exchange on garnet surface for the stable lithium-solid electrolyte interface. *ACS Applied Materials & Interfaces*, 11: 35030–35038.

[88] Cai, M. L., Lu, Y., Yao, L., Jin, J., Wen, Z. Y. (2021). Robust conversion-type Li/garnet interphases from metal salt solutions. *Chemical Engineering Journal*, 417: 129158.

[89] Zheng, H. P., Wu, S. P., Tian, R., Xu, Z. M., Zhu, H., Duan, H. N., Liu, H. Z. (2020). Intrinsic lithiophilicity of Li–garnet electrolytes enabling high-rate lithium cycling. *Advanced Functional Materials*, 30: 1906189.

[90] Wu, J. F., Pu, B. W., Wang, D., Shi, S. Q., Zhao, N., Guo, X. X., Guo, X. (2019). In situ formed shields enabling Li_2CO_3-free solid electrolytes: A new route to uncover the intrinsic lithiophilicity of garnet electrolytes for dendrite-free Li-metal batteries. *ACS Applied Materials & Interfaces*, 11: 898–905.

[91] Ruan, Y. D., Lu, Y., Li, Y. P., Zheng, C. J., Su, J. M., Jin, J., Xiu, T. P., Song, Z., Badding, M. E., Wen, Z. Y. (2020). A 3D cross-linking lithiophilic and electronically insulating interfacial engineering for garnet-type solid-state lithium batteries. *Advanced Functional Materials*, 31: 2007815.

[92] Xu, R., Liu, F., Ye, Y. S., Chen, H., Yang, R. R., Ma, Y. X., Huang, W. X., Wan, J. Y., Cui, Y. (2021). A morphologically stable Li/electrolyte interface for all-solid-state batteries enabled by 3D-micropatterned garnet. *Advanced Materials*, 33: e2104009.

[93] Ruan, Y. D., Lu, Y., Li, Y. P., Zheng, C. J., Su, J. M., Jin, J., Xiu, T. P., Song, Z., Badding, M. E., Wen, Z. Y. (2021). A 3D cross-linking lithiophilic and electronically insulating interfacial engineering for garnet-type solid-state lithium batteries. *Advanced Functional Materials*, 31: 2007815.

[94] Ji, X., Hou, S., Wang, P. F., He, X. Z., Piao, N., Chen, J., Fan, X. L., Wang, C. S. (2020). Solid-state electrolyte design for lithium dendrite suppression. *Advanced Materials*, 32: e2002741.

[95] Xu, H. J., Cao, G. Q., Shen, Y. L., Yu, Y. R., Hu, J. H., Wang, Z., Shao, G. S. (2021). Enabling argyrodite sulfides as superb solid-state electrolyte with remarkable interfacial stability against electrodes. *Energy & Environmental Materials*, https://doi.org/10.1002/eem2.12282.

[96] Zhao, F., Sun, Q., Yu, C., Zhang, S., Adair, K., Wang, S., Liu, Y., Zhao, Y., Liang, J., Wang, C., et al. (2020). Ultrastable anode interface achieved by fluorinating electrolytes for all-solid-state Li metal batteries. *ACS Energy Letters*, 5: 1035–1043.

[97] Liu, Y., Su, H., Li, M., Xiang, J. Y., Wu, X. Z., Zhong, Y., Wang, X. L., Xia, X. H., Gu, C. D., Tu, J. P. (2021). In situ formation of a Li_3N-rich interface between lithium and argyrodite solid electrolyte enabled by nitrogen doping. *Journal of Materials Chemistry A*, 9: 13531–13539.

[98] Li, Y. T., Chen, X., Dolocan, A., Cui, Z. M., Xin, S., Xue, L. G., Xu, H. H., Park, K., Goodenough, J. B. (2018). Garnet electrolyte with an ultralow interfacial resistance for Li-metal batteries. *Journal of the American Chemical Society*, 140: 6448–6455.

[99] Huo, H. Y., Gao, J., Zhao, N., Zhang, D. X., Holmes, N. G., Li, X. N., Sun, Y. P., Fu, J. M., Li, R. Y., Guo, X. X., et al. (2021). A flexible electron-blocking interfacial shield for dendrite-free solid lithium metal batteries. *Nature Communications*, 12: 176.

[100] Cheng, Z. Y., Xie, M. L., Mao, Y. Y., Ou, J. X., Zhang, S. J., Zhao, Z., Li, J. L., Fu, F., Wu, J. H., Shen, Y. B., et al. (2020). Building lithiophilic ion-conduction highways on garnet-type solid-state Li^+ conductors. *Advanced Energy Materials*, 10: 1904230.

[101] Hitz, G. T., McOwen, D. W., Zhang, L., Ma, Z. H., Fu, Z. Z., Wen, Y., Gong, Y. H., Dai, J. Q., Hamann, T. R., Hu, L. B., et al. (2019). High-rate lithium cycling in a scalable trilayer Li-garnet-electrolyte architecture. *Materials Today*, 22: 50–57.

[102] Wan, H. L., Liu, S. F., Deng, T., Xu, J. J., Zhang, J. X., He, X. Z., Ji, X., Yao, X. Y., Wang, C. S. (2021). Bifunctional interphase-enabled $Li_{10}GeP_2S_{12}$ electrolytes for lithium–sulfur battery. *ACS Energy Letters*, 6: 862–868.

[103] Zhang, Z. X., Zhang, L., Yan, X. L., Wang, H. Q., Liu, Y. Y., Yu,

C., Cao, X. T., van Eijck, L., Wen, B. (2019). All-in-one improvement toward Li_6PS_5Br-based solid electrolytes triggered by compositional tune. *Journal of Power Sources,* 410–411: 162–170.

[104] Li, H. M., Yin, H. Y., Wang, K. L., Cheng, S. J., Jiang, K., Sadoway, D. R. (2016). Liquid metal electrodes for energy storage batteries. *Advanced Energy Materials*, 6: 1600483.

[105] Hueso, K. B., Armand, M., Rojo, T. (2013). High temperature sodium batteries: Status, challenges and future trends. *Energy & Environmental Science*, 6: 734–749.

[106] Lu, X. C., Li, G. S., Kim, J. Y., Mei, D. H., Lemmon, J. P., Sprenkle, V. L., Liu, J. (2014). Liquid-metal electrode to enable ultra-low temperature sodium–beta alumina batteries for renewable energy storage. *Nature Communications*, 5: 4578.

[107] Gross, M. M., Percival, S. J., Lee, R. Y., Peretti, A. S., Spoerke, E. D., Small, L. J. (2021). A high-voltage, low-temperature molten sodium battery enabled by metal halide catholyte chemistry. *Cell Reports Physical Science*, 2: 100489.

[108] Jin, Y., Liu, K., Lang, J. L., Zhuo, D., Huang, Z. Y., Wang, C. G., Wu, H., Cui, Y. (2018). An intermediate temperature garnet-type solid electrolyte-based molten lithium battery for grid energy storage. *Nature Energy*, 3: 732–738.

[109] Bradwell, D. J., Kim, H., Sirk, A. H. C., Sadoway, D. R. (2012). Magnesium-antimony liquid metal battery for stationary energy storage. *Journal of the American Chemical Society*, 134: 1895–1897.

[110] Wang, K. L., Jiang, K., Chung, B., Ouchi, T., Burke, P. J., Boysen, D. A., Bradwell, D. J., Kim, H., Muecke, U., Sadoway, D. R. (2014). Lithium–antimony–lead liquid metal battery for grid-level energy storage. *Nature*, 514: 348–350.

[111] Li, H. M., Wang, K. L., Cheng, S. J., Jiang, K. (2016). High performance liquid metal battery with environmentally friendly antimony-tin positive electrode. *ACS Applied Materials & Interfaces*, 8: 12830–12835.

[112] Yan, S., Zhou, X. B., Li, H. M., Shen, Y., He, Y. L., Zhou, H., Wang, K. L., Jiang, K. (2021). Utilizing in situ alloying reaction to achieve the self-healing, high energy density and cost-effective Li||Sb liquid metal battery. *Journal of Power Sources*, 514: 230578.

[113] Ning, X. H., Phadke, S., Chung, B., Yin, H. Y., Burke, P., Sadoway, D. R. (2015). Self-healing Li-Bi liquid metal battery for grid-scale energy storage. *Journal of Power Sources*, 275: 370–376.

[114] Dai, T., Zhao, Y., Ning, X. H., Narayan, R. L., Li, J., Shan, Z. W. (2018). Capacity extended bismuth-antimony cathode for high-performance liquid metal battery. *Journal of Power Sources*, 381: 38–45.

[115] Zhao, W., Li, P., Liu, Z. W., He, D. L., Han, K., Zhao, H. L., Qu, X. H. (2018). High-performance antimony–bismuth–tin positive electrode for liquid metal battery. *Chemistry of Materials*, 30: 8739–8746.

[116] Li, H. M., Wang, K. L., Zhou, H., Guo, X. L., Cheng, S. J., Jiang, K. (2018). Tellurium-tin based electrodes enabling liquid metal batteries for high specific energy storage applications. *Energy Storage Materials*, 14: 267–271.

[117] Ouchi, T., Kim, H., Spatocco, B. L., Sadoway, D. R. (2016). Calcium-based multi-element chemistry for grid-scale electrochemical energy storage. *Nature Communications*, 7: 10999.

[118] Ding, Y., Guo, X. L., Qian, Y. M., Yu, G. H. (2020). Low-temperature multielement fusible alloy-based molten sodium batteries for grid-scale energy storage. *ACS Central Science*, 6: 2287–2293.

[119] Ding, Y., Guo, X. L., Qian, Y. M., Xue, L. G., Dolocan, A., Yu, G. H. (2020). Room-temperature all-liquid-metal batteries based on fusible alloys with regulated interfacial chemistry and wetting. *Advanced Materials*, 32: e2002577.

[120] Ding, Y., Guo, X., Qian, Y., Zhang, L., Xue, L., Goodenough, J. B., Yu, G. (2019). A liquid-metal-enabled versatile organic alkali-ion battery. *Advanced Materials*, 31: e1806956.

[121] Ahlbrecht, K., Bucharsky, C., Holzapfel, M., Tübke, J., Hoffmann, M. J. (2017). Investigation of the wetting behavior of Na and Na alloys on uncoated and coated Na-β" -alumina at temperatures below 150 ºC. *Ionics*, 23: 1319–1327.

[122] Chang, H. J., Lu, X. C., Bonnett, J. F., Canfield, N. L., Han, K., Engelhard, M. H., Jung, K., Sprenkle, V. L., Li, G. S. (2018). Decorating β"-alumina solid-state electrolytes with micron Pb spherical particles for improving Na wettability at lower temperatures. *Journal of Materials Chemistry A*, 6: 19703–19711.

[123] Jin, D. N., Choi, S., Jang, W., Soon, A., Kim, J., Moon, H., Lee, W., Lee, Y., Son, S., Park, Y. C., et al. (2019). Bismuth Islands for low-temperature sodium-beta alumina batteries. *ACS Applied Materials & Interfaces*, 11: 2917–2924.

[124] Li, G. S., Lu, X. C., Kim, J. Y., Lemmon, J. P., Sprenkle, V. L. (2014). Improved cycling behavior of ZEBRA battery operated at intermediate temperature of 175 ºC. *Journal of Power Sources*, 249: 414–417.

[125] Hu, Y. Y., Wen, Z. Y., Wu, X. W., Lu, Y. (2013). Nickel nanowire network coating to alleviate interfacial polarization for Na-beta battery applications. *Journal of Power Sources*, 240: 786–795.

[126] Hu, Y. Y., Wen, Z. Y., Wu, X. W. (2014). Porous iron oxide coating on β"-alumina ceramics for Na-based batteries. *Solid State Ionics*, 262: 133–137.

[127] Jin, D. N., Lee, H. G., Choi, S., Kim, S., Lee, Y., Son, S., Park, Y. C., Lee, J. S., Jung, K., Shim, W. (2019). Sparked reduced graphene oxide for low-temperature sodium-beta alumina batteries. *Nano Letters*, 19: 8811–8820.

[128] Li, M. M., Lu, X. C., Zhan, X. W., Engelhard, M. H., Bonnett, J. F., Polikarpov, E., Jung, K., Reed, D. M., Sprenkle, V. L., Li, G. S. (2021). High performance sodium-sulfur batteries at low temperature enabled by superior molten Na wettability. *Chemical Communications*, 57: 45–48.

[129] Gross, M. M., Small, L. J., Peretti, A. S., Percival, S. J., Rodriguez, M. A., Spoerke, E. D. (2020). Tin-based ionic chaperone phases to improve low temperature molten sodium–NaSICON interfaces. *Journal of Materials Chemistry A*, 8: 17012–17018.

[130] Jin, Y., Liu, K., Lang, J. L., Jiang, X., Zheng, Z. K., Su, Q. H., Huang, Z. Y., Long, Y. Z., Wang, C. G., Wu, H., et al. (2020). High-energy-density solid-electrolyte-based liquid Li-S and Li-Se batteries. *Joule*, 4: 262–274.

[131] Lang, J. L., Liu, K., Jin, Y., Long, Y. Z., Qi, L. H., Wu, H., Cui, Y. (2020). A molten battery consisting of Li metal anode, $AlCl_3$-LiCl cathode and solid electrolyte. *Energy Storage Materials*, 24: 412–416.

[132] Xu, J., Liu, K., Jin, Y., Sun, B., Zhang, Z. L., Chen, Y., Su, D. W., Wang, G. X., Wu, H., Cui, Y. (2020). A garnet-type solid-electrolyte-based molten lithium-molybdenum-iron(II) chloride battery with advanced reaction mechanism. *Advanced Materials*, 32: e2000960.

[133] Liu, K., Lang, J. L., Yang, M. Z., Xu, J., Sun, B., Wu, Y. L., Wang, K. Y., Zheng, Z. K., Huang, Z. Y., Wang, C. G., et al. (2020). Molten lithium-brass/zinc chloride system as high-performance and low-cost battery. *Matter*, 3: 1714–1724.

[134] Kim, H., Boysen, D. A., Newhouse, J. M., Spatocco, B. L., Chung, B., Burke, P. J., Bradwell, D. J., Jiang, K., Tomaszowska, A. A., Wang, K. L., et al. (2013). Liquid metal batteries: Past, present, and future. *Chemical Reviews*, 113: 2075–2099.

[135] Kim, J., Shin, D., Jung, Y., Hwang, S. M., Song, T., Kim, Y., Paik, U. (2018). LiCl-LiI molten salt electrolyte with bismuth-lead positive electrode for liquid metal battery. *Journal of Power Sources*, 377: 87–92.

[136] Yu, H., Lu, H. M., Hu, X. Q., Liu, J. X., Cao, Y. (2020). LiI-KI and LAGP electrolytes with a bismuth-tin positive electrode for the development of a liquid lithium battery. *Materials Chemistry and Physics*, 247: 122865.

[137] Lalau, C., Dimitrova, A., Himmerlich, M., Ispas, A., Weier, T., Krischok, S., Bund, A. (2016). An electrochemical and photoelectron spectroscopy study of a low temperature liquid metal battery based on an ionic liquid electrolyte. *Journal of the Electrochemical Society*, 163: A2488–A2493.

[138] Meng, X. C., Zuo, G. Z., Xu, W., Sun, Z., Huang, M., Yuan, X. L., Xu, C., Hu, W. Y., Andruczyk, D., Hu, J. S., et al. (2018). Effect of temperature on the corrosion behaviors of 304 stainless steel in static liquid lithium. *Fusion Engineering and Design*, 128: 75–81.

[139] Tsisar, V., Kondo, M., Xu, Q., Muroga, T., Nagasaka, T., Yeliseyeva, O. (2011). Effect of nitrogen on the corrosion behavior of RAFM JLF-1 steel in lithium. *Journal of Nuclear Materials*, 417(1–3): 1205–1209.

[140] Cui, K. X., An, F. Q., Zhao, W., Li, P., Li, S. W., Liu, C. R., Qu, X. H. (2021). Feasibility research of SS304 serving as the positive current collector of Li||Sb-Sn liquid metal batteries. *The Journal of Physical Chemistry C*, 125: 237–245.

[141] Ouchi, T., Sadoway, D. R. (2017). Positive current collector for Li||Sb-Pb liquid metal battery. *Journal of Power Sources*, 357: 158–163.

[142] Cui, K. X., Zhao, W., Zhou, D. M., Li, S. W., Liu, C. R., Li, P., Qu, X. H. (2021). Stable positive current collectors for Li||Sb–Sn liquid metal batteries. *ACS Applied Energy Materials*, 4: 9013–9021.

[143] Baker, D. J., Bugden, W. G., Smith, P. R. (1991). Joining of ceramic components to metal components. US Patent, US5009357A.

[144] Nagura, M., Kondo, M., Suzuki, A., Muroga, T., Terai, T. (2007). Experimental study on corrosion of ceramic materials in natural convection lithium loop. *Fusion Science and Technology*, 52: 630–634.

[145] Terai, T., Suzuki, A., Yoneoka, T., Mitsuyama, T. (2000). Compatibility of AlN with liquid lithium. *Journal of Nuclear Materials*, 283–287: 1322–1325.